1989

Fluidization of granular media in unbounded two-dimensional domains: numerical calculations of incipient conditions, 70p (no date but assume 1989)

Gerard P. Lennon

F. Tom Chang

FLUIDIZATION OF GRANULAR MEDIA IN UNBOUNDED TWO-DIMENSIONAL DOMAINS: NUMERICAL CALCULATIONS OF INCIPIENT CONDITIONS

by

Gerard P. Lennon and F. Tom Chang

Lehigh University

Bethlehem, PA 18015

IMBT Hydraulics Lab Report #IHL-124-89

ABSTRACT

From the theory of flow through porous media, the governing equation for hydraulic head is developed for flow emanating from small holes in a pipe buried in fine sand in the coastal environment. The head distribution in the domain is obtained from the two-dimensional finite element method and validated with experimental results. The theoretical critical hydraulic gradient is used to predict the incipient fluidization flow rate conditions for the available experimental data as well as for selected field situations. Numerous simulations for a wide range of expected conditions are then incorporated into practical fluidization system design charts.

1.0 INTRODUCTION

1.1 Traditional Applications of Fluidization

One-dimensional fluidization has been applied to a wide variety of traditional applications in areas such as heat transfer, petroleum refining, petrochemical processing, coal conversion, ore roasting, coking, aluminum production, and production of a variety of chemical compounds (Wen and Yu, 1966; Roberts et al., 1986). Intentional one-dimensional fluidization often results from a well-distributed source of upflowing fluid under a bed of solid particles confined by lateral boundaries. As fluid flows upward, head loss occurs through the bed as a result of viscous and inertial effects. For one-dimensional problems the superficial velocity (specific discharge), V, is the upward volumetric flow rate divided by the total cross-sectional area of the fluidized domain. The minimum V causing fluidization is V_i, occurring when the upward drag equals the submerged weight of the particles.

Extensive work on one-dimensional fluidization has allowed the development of the theoretical minimum fluidization velocity, V_i (Wen and Yu, 1966). Additional research has improved the application to design of such processes as rapid sand filter backwashing (Amirtharajah, 1970; Amirtharajah and

Cleasby, 1972; and Cleasby and Fan, 1981).

For Reynolds numbers, R, less than 3 the head loss through the fixed bed is a linear function of the flow rate,

$$V = KJ \qquad (1.1)$$

where K is the hydraulic conductivity (coefficient of permeability) and J is the hydraulic gradient. Here $R = \rho V d_{eq}/\mu$, d_{eq} = grain diameter of a sphere of equal volume, μ = dynamic viscosity of water. Camp (1964) has reported strictly laminar flow through filters up to R = 6. A number of predictive equations are available for nonlinear flow, including Irmay's (1958) analysis summarized in Appendix 1.

Applications of fluidization to unbounded domains in the coastal environment are presented in references such as Weisman and Collins (1979) and Parks et al. (1983). Descriptions of two-dimensional laboratory experiments are available in Kelley (1977), Roberts et al. (1986), and more recently by Clifford (1989). These experiments include pre-, incipient and post-fluidization data. Weisman et al. (1988) summarized Roberts et al.'s (1986) experiments, with emphasis on the processes occurring after fluidization.

1.2 Application to the Coastal Environment

The present application considers a source pipe buried in or near a tidal inlet for the purpose of maintaining a channel as an alternative to dredging or to aid in sand bypassing. The formation of both fluidized and unfluidized regions creates a complicated geometry, with a portion of the flow entering the unfluidized zone. In a one-dimensional problem, the specific discharge (superficial velocity), V, and head gradient, J, are constant in the domain. However, in the present application the flow diverges from holes in a source pipe with largest gradient nearest the holes.

For grain sizes tidal found near inlets (generally less than 0.5 mm according to Bruun and Gerritsen, 1959) and the fluidization system described here, Reynolds numbers typically do not exceed 1 except in the immediate vicinity of the source pipe. Unlike many applications of fluidization, Darcy's law can be used, i.e. inertia and turbulence can be ignored up to and including incipient fluidization.

The objective of the present study is to predict Q_i, the superficial fluid flow rate required to initiate fluidization of a bed of fine sand for a pipe buried in the coastal environment. The theory of flow through porous media is used to determine h, the hydraulic head distribution. The governing

differential equation and boundary conditions for h are approximated numerically using the finite element method (FEM). The model is validated with Roberts et al.'s (1986) experimental data and an alternate numerical method. Once validated, the FEM is used to analyze conditions not analyzed experimentally. Numerous simulations for a wide range of expected conditions are then incorporated into practical fluidization system design charts.

2.0 RANGE OF VALIDITY OF DARCY'S LAW

Darcy's Law (Eq. 1.1) is valid if the Darcy velocity, V, is linearly related to the hydraulic gradient, J. Bear (1972) and Davidson et al. (1985) present numerous equations that can be applied to pre- and incipient fluidization when Darcy's Law is not valid. Many equations can be expressed in Forchheimer's empirical form.

$$J = AV + BV^2 \qquad (2.1)$$

where A and B are coefficients to be determined (Bear, 1972). The second term in Eq. 2.1 is negligible compared to the first for low Reynolds numbers, resulting in Darcy's Law with A = 1/K where K is the hydraulic conductivity. Irmay's (1958) one-dimensional equation is used to calculate A and B in Eq. 2.1 for various grain sizes as described in Appendix 1. Figure 2.1 shows the variation of hydraulic gradient with the Reynolds number for selected grain sizes. Incipient fluidization is limited by J = 1.02 (top of Fig. 2.1) as discussed in the next section. Smaller grain sizes have lower values of maximum J and R at the incipient condition. For sand grain sizes normally found near tidal inlets (0.2 mm to 0.5 mm according to Bruun and Gerritsen, 1959) the Reynolds number is less than 1 as shown in Fig. 2.1.

2.1 Experimental Data of Roberts et al. (1986)

Roberts et al. (1986) obtained head data for a number of prefluidization flow rates for each of two bed depths. Flow emanated from perforations in a source pipe of diameter D buried a depth d_b as shown in Fig. 2.2. Fine sand was chosen because it has the size, shape, and consistency of material found in the coastal environment, especially in or near tidal inlets. The sand had a specific gravity of 2.67, compacted porosity of 39%, d_{50} = 0.15 mm ,and d_{90} = 0.21 mm. The line labeled 0.15 mm in Fig. 2.1 corresponds to the d_{50} of Roberts et al. (1986).

For low flow rates, the bed remained unfluidized. As the flow rate was slowly increased in discrete increments, a local boil (spout) on the sand surface occurred above the pipe. A slight increase in flow rate resulted in enlarged boils that coalesced until the bed above the supply pipe was fluidized along its entire length. The transition from an unfluidized to a completely fluidized bed was observed to be a rather unstable phenomena. Couderc (1985) suggests that fluidization occurs over a range of velocities accounting for different particle sizes. The particle distribution is fairly narrow for Roberts et al.'s (1986) sand, resulting in a narrow range of required flow rate to fluidize different sand grain sizes in the bed.

Up to incipient fluidization, almost half of the flow is into areas that won't fluidize even at much higher flow rates. Because of this "leakage", the flow rate required to initiate fluidization is greater than the one-dimensional analog, i.e. a domain bounded directly below and close to the sides of the source pipe that restricts flow to be essentially upward.

Unlike one-dimensional theory, the diverging flow of Roberts et al.'s (1986) test apparatus created a situation whereby the gradient varied throughout the bed. An analysis Roberts et al.'s (1986) data indicates that the average critical gradients were 1.06 and 1.10 for the 25.4 cm and 42 cm bed depths, respectively. Table 2.1 presents the distribution of gradient in a vertical line almost directly above the source pipe for the 42 cm bed depth at approximately incipient flow. The average critical gradient from just above the pipe to the surface of the sand was calculated by dividing the change in head by the distance between the taps, i.e. the weighted average of the entries in Column 4 of Table 2.1. A simple one-dimensional force-balance theory (Peck et al., 1974) predicts $i_c = (\rho_s - \rho_w)/\rho_w$, = 1.02 for this sand.

The gradient of 1.25 reported by Roberts et al. (1986) is based on the gradient in the lower 22 cm of the 42 cm bed. This value is obtained by a weighted average of the last 3 entries in Column 4 of Table 2.1. If the upper 33 cm of the bed

is used to calculate the gradient (above tap 29), the gradient is 0.98, below the theoretical gradient.

The Reynolds number was computed at the tap locations for Roberts et al.'s (1986) experimental data, using $d_{eq} = d_{50}$. The highest calculated Reynolds numbers was 0.05 for the tap closest to the pipe; at most locations the Reynolds number was on the order of 10^{-3} or 10^{-4}. Additional experiments are being conducted to determine gradients, velocities and Reynolds numbers closer to the source pipe.

Roberts et al. (1986) experimentally determined the horizontal hydraulic conductivity to be K = 0.018 cm/s in a two-dimensional flow model with virtually horizontal flow over a four foot distance between vertical reservoirs. K was to be 0.008 cm/sec when compacted using a constant head permeameter. The first value may be more reflective of the horizontal value, whereas the second may be appropriate for the vertical hydraulic conductivity. The harmonic mean, square root of $(K_x K_y)$, is 0.012 cm/s, in good agreement with the predicted value of 0.0125 obtained by Irmay's Equation (Appendix 1).

3.0 FINITE ELEMENT ANALYSIS OF PRE- AND INCIPIENT FLUIDIZATION

3.1 INTRODUCTION

The finite element method (FEM) was used to analyze two-dimensional pre- and incipient fluidization behavior. The theoretical considerations of the finite element method are discussed here in Section 3. The user's manual provided in Appendix 2 summarizes additional details of the actual algorithms used in the model.

The finite element method was chosen as the numerical method to simulate pre- and incipient fluidization behavior. Representation of the source holes would be difficult with the finite difference method, even if a variable grid were employed. Other techniques such as the boundary element method (BEM) are easier to apply to isotropic, homogeneous media than the FEM. The FEM was chosen for the analyses here because it is more powerful; only minor changes are needed to account for anisotropic, nonhomogeneous, nonlinear flow.

Lennon (1986) used two-dimensional finite element method (FEM) results to validate boundary element method (BEM) results for a problem of variable pressures on a completely impermeable pipe buried in the sand. The present application is very

similar to the Lennon (1986) case except for a difference in boundary conditions. The use of two separate models minimizes the possibility of errors in the model and/or the data set, and well as providing an estimate of the approximation of accuracy of the techniques.

3.2 VALIDATION WITH THE BOUNDARY ELEMENT METHOD

Figure 3.1 presents the validation of the finite element model (FEM) with the boundary element model (BEM) for a test case (Simulation 1). The predicted head distributions vary slightly because the boundary element method solves the governing differential equation exactly in the domain whereas the FEM approximates the governing equations. Also, a slight difference in handling the source hole configuration leads to slight differences. Similar minor differences were observed by Lennon (1986).

No change to these codes are required when Darcy's Law is valid; changes were restricted type of boundary conditions combined with a new computational grid refined in the vicinity of the the source pipe. A postprocessing routine was added that calculated the flow rate factor (Q_i/Kd_b), the average vertical gradient above the bed, and an improved hydraulic head contouring routine. A separate nonlinear flow version of the

program is being developed that uses Eq. 2.1 in place of Darcy's Law for cases where inertia terms are important. The results were carried out using a FORTRAN F77 compiler on a UNIX workstation driven by a 16 Mhz Motorola 68020 chip. Finite element run times were on the order of 3 minutes for each simulation using a 1055 element, 584 node grid.

3.3 THEORETICAL FORMULATION

For sandy soils where fluidization does not occur and inertia terms are negligible, Darcy's Law can be used. If the Reynolds number is high enough, Eq. 1.1 is used in place of Darcy's Law; however for the results and formulation presented here, Darcy's Law was assumed to be valid. Assuming that the flow rate is increased slowly allows the system to be analyzed as a steady flow problem.

Combining Darcy's Law with the continuity equation results in the equation governing the hydraulic head distribution in the domain,

$$L(h) = \frac{\partial}{\partial x}\left(K_x \frac{\partial h}{\partial x}\right) + \frac{\partial}{\partial y}\left(K_y \frac{\partial h}{\partial y}\right) = 0 \qquad (3.1)$$

for steady state conditions. The associated boundary conditions are $h = 0$ on the soil surface, and $\partial h/\partial n = 0$ on the source pipe, impermeable bottom, and impermeable side walls as shown in Fig. 2.2.

3.4 FINITE ELEMENT METHOD

The finite element technique is similar to that used by Liu and Lennon (1978) and Lennon (1986). The governing equation (Eq. 3.1) is transformed into integral form using the method weighed residuals. The solution domain is divided into triangular finite elements (see Fig. 3.1) and the head is approximated within each element by

$$\hat{h} = \{N\}^T \{h\}_e \qquad (3.2)$$

where $\{N\}$ is a vector of three linearly independent basis functions defined over each element and $\{h_e\}$ is a vector of the approximate pressure at each node (corner of the triangular element). Because $\hat{h}$ is only an approximation to $h(x,z)$, then $L(\hat{h}) = r = 0$ where r is a residual associated with the solution. Using the Galerkin method, the weighed average of the residuals over the whole domain is set to zero. Global

equations are formed that can be written as [K]{h} = {R} where [K] is a known coefficient matrix, {h} is the matrix of approximate head values at every node in the domain, and {R} is a known right hand side that includes the information associated with the boundary conditions (Liu and Lennon, 1978). The solution for {h} is obtained by a standard equation solving routine (Liu and Lennon, 1978).

The finite element method as used in this report is essentially the same procedure presented earlier by Liu and Lennon (1978).

3.5 Validation Simulations

Figure 3.2 presents the validation of the finite element model (FEM) with Roberts et al.'s (1986) Test 2 head data for a flow rate of 0.0344 l/s-m (10.45 cc/s), about 40 percent of the incipient flow rate. The FEM contours were obtained using an isotropic value of K = 0.012 cm/s. The finite element grid was obtained by rescaling the 1055 element shown in Fig. 3.3. The predicted head distribution generally agrees within 1 cm of head at the observed points. The experimental head value just to the right of the pipe at (x,y) = (9.6 cm, 1.6 cm) may still be within the zone where the three-dimensional nature of the jets has not completely spread over the experimental tank width

of 30.48 cm. The validation of the model using these data is adequately demonstrated using this value of K.

Additional simulations were conducted for other values of hydraulic conductivity. Figures 3.4 through 3.8 were conducted with values of K of:

Figure Number	K_x, cm/s	K_y, cm/s
3.4	0.014	0.012
3.5	0.016	0.012
3.6	0.018	0.012
3.7	0.018	0.008
3.8	0.02	0.01

For a slightly higher flow rate and K_y = 0.008 cm/s, Figs. 3.9 and 3.10 show the match using K_x = 0.018 and 0.02 cm/s, respectively. The isotropic conditions simulation (Fig. 3.2) appears to reproduce the observed contours the best.

3.6 Predictive Simulations

A deeper burial depth will require a larger incipient fluidization flow rate because the flow distances are greater and the gradient is approximately the same. In addition, the required flow rate should increase linearly with an increase in hydraulic conductivity. The theoretical gradient of 1.02 is used in the predictive calculations over the upper 95% of the burial depth.

The first simulation was conducted using the grid shown in Fig. 3.11 for a unit pipe diameter (D = 1 unit). The other geometrical quantities appearing are the burial depth $d_b/D = 20$ and the distances to the impervious boundaries $X_d/D = 100$, $Y_d/D = 60$ (see Fig. 2.2). For the case of D = 1 ft (0.305 m), the hydraulic head contours obtained with the FEM are shown in Fig. 3.12.

The maximum hydraulic head, h_{max}, at the hole in the pipe was calculated to be 40.35 ft (12.3 m); the value of h_{max}/d_b is about 2. If the the theoretical one-dimensional critical hydraulic gradient (1.02) is multiplied by the depth of burial alone, a value of about half this number is obtained. This difference occurs because the flow has significant horizontal components, tending to spread out. The soil that eventually fluidizes feels the effects of the highly concentrated flow,

but it is diffused by lower surrounding values of head. Inspection Fig. 3.12 shows that about half of the 40.35 ft of head loss occurs in the immediate vicinity of the pipe, i.e. the 20 ft contour is very close to the pipe.

Simulations were run for depths d_b = 5 to 40 ft, domain widths from X_d = 50 to 3000 ft, and domain depths Y_d = 20 to 240 ft. The largest domain size provides a good approximation of an infinite domain. The design chart for eighth-inch diameter holes is provided in Fig. 3.13a, showing variation of flow rate factor (Q_i/Kd_b) versus d_b for isotropic conditions; graphs for an anisotropic value of K_x/K_y = 10 is presented in Figure 3.13b.

Although larger domains require larger flow rates, the gradient above the pipe only varies slightly; h_{max}/d_b is about 2 where h_{max} is the head at the source pipe holes. Additional simulations are being conducted to determine the importance of possible non-linear flow in the immediate vicinity of the source pipe. Table 3.1 summarizes the range of h_{max}/d_b for the simulations run here.

4.0 CONCLUSIONS

The main conclusions of this investigation were:

1. The required incipient fluidization flow rate can be obtained from numerical simulation of flow through porous media.

2. The finite element model was validated with Roberts et al. (1986) hydraulic head and gradient data.

3. Predictive simulations provide estimates of the required flow rates needed to initiate fluidization in situations impractical to verify in the laboratory.

4. Figures 3.13a and 3.13b are useful charts for the design flow rate for fluidization systems in the coastal environment for isotropic conditions and a 10:1 anisotropic value of horizontal to vertical hydraulic conductivity.

5. The head loss is about twice the burial depth at incipient conditions, about twice that predicted by one-dimensional theory.

The design charts provided in this report do not take into

account possible design considerations such as algae fouling, clogging of fluidization holes, nonlinear flow, or three-dimensional effects that conflict with the assumptions of the problems (such a variable distribution of pressure inside the fluidization pipe), and variations in the properties of the porous medium.

5.0 FUTURE WORK

Additional experimental data are being obtained to define the nearfield head distribution in the vicinity of the source pipe, and a three-dimensional numerical model will be validated with those data. A nonlinear flow model is being developed to assess the nonlinear flow effects in the vicinity of the source pipe. The nonlinear flow model will be validated with supplementary experimental data to be obtained in the future.

6.0 ACKNOWLEDGEMENTS

A portion of the funding for this work was provided by the U.S. Army Corps of Engineers, Dredging Research Program. The authors would also like to thank Dr. Irwin J. Kugelman, Director of the Environmental Studies Center, Lehigh University for aiding in the support of this study.

7.0 REFERENCES

Amirtharajah, A. (1970). "Expansion of Graded Sand Filters During Backwashing," Master of Science Thesis, Iowa State University, Ames, Iowa.

Amirtharajah, A., and Cleasby, J. L. (1972). "Prediction of Expansion of Filters During Backwash," J. Amer. Water Works Assoc., 64, 47-52.

Bear, J. (1972). Dynamics of Fluids in Porous Media, American Elsevier, New York.

Bruun, P.F., and Gerritsen (1959). "Natural Bypassing of Sand at Coastal Inlets," J. of Amer. Soc. of Civil Engineers, 85, 75-107.

Camp, T. R. (1964). "Theory of Water Filtration". Journal of the Sanitary Engineering Division ASCE, 48(SA4) Proc. Paper, 1-30.

Chang, T. F-C., Lennon, G. P., Weisman, R. N. and Du, B. L. (1989). "Predicting 2-D Pre- and Incipient Fluidization By 1-D Theory," Proceedings of the Third National Conference on Hydraulic Engineering, New Orleans, August 14-18, (in press).

Couderc, J-P., (1985). "Incipient Fluidization and Particulate Systems," in Fluidization, edited by J. F. Davidson, R. Clift and D. Harrison, 2nd ed., Academic Press, 7-23.

Cleasby, J. L. and Fan, K. S. (1981). "Predicting Fluidization and Expansion of Filter Media". Journal of Environmental Engineering Division, ASCE, 107(EE3), 455-471.

Clifford, J., (1989). "Slurry Removal From the Fluidized Region of an Unbounded Domain: An Experimental Study," Master of Science Thesis, Lehigh University, Bethlehem, PA.

Davidson, J. F., Clift, R., Harrison, D. (editors), (1985). Fluidization, 2nd ed., Academic Press.

Fan, K-S. (1978). "Sphericity and Fluidization of Granular Filter Media," Master of Science Thesis, Iowa State University, Ames, Iowa.

Irmay, S. (1958). "On the Theoretical Derivation of Darcy and Forchheimer Formulas," Eos Trans., AGU, 39, 702-707.

Kelley, J. T., (1977). "Fluidization Applied to Sediment Transport, Master of Science Thesis, Lehigh University, Bethlehem, PA.

Lennon, G. P. (1986). "A Boundary Element Package Developed for Three-dimensional Wave-Induced Forces on Buried Pipelines, Conference Proceedings, BETECH '86: The Boundary Element Technology Conference, June 1986, 359-368.

Liu, P. L-F., and Lennon, G. P. (1978). "Finite Element Modeling of Nearshore Currents," Journal of Waterway, Port, Coastal and Ocean Division, ASCE, 104(WW2), 175-189.

Parks, J. M., Weisman, R. N., and Collins, A. G. (1983). "Fluidization Applied to Sediment Transport (FAST) as an Alternative to Maintenance Dredging of Navigation Channels in Tidal Inlets," Wastes in the Ocean, Volume II: Dredged Material Disposal in the Ocean, ed. D. R. Kester, B. H. Ketchum, I. W. Duedall, and P. K. Park, John Wiley and Sons, Inc.

Peck, R. B., Hanson, W. E., and Thornburn, T. H. (1974). Foundation Engineering, John Wiley and Sons, Inc.

Roberts, E. W., Weisman, R. N., and Lennon, G. P. (1986). "Fluidization of Granular Media in Unbounded Two-Dimensional Domains: An Experimental Study," Imbt Hydraulics Lab Report No. IHL-109-86, Lehigh University, Bethlehem, PA.

Weisman, R. N. and Collins, A. G. (1979). Stabilization of Tidal Inlet Channels--Design Recommendations. Fritz Engineering Lab Report No. 710.3, Lehigh University, Bethlehem, PA.

Weisman, R. N., Collins, A. G. and Parks, J. M. (1982). "Maintaining Tidal Inlet Channels by Fluidization". Journal of the Waterway Port, Coastal, and Ocean Division, ASCE, 108(WW4), 526-538.

Weisman, R.N., Lennon, G.P., and Roberts, E. W. (1988). "Experiment on Fluidization in Unbounded Domains," Journal of Hydraulic Engineering, ASCE, 114(5), 502-515.

Wen, C. Y. and Yu, Y. H. (1966). "Mechanics of Fluidization". Chemical Engineering Prog. Symp. Series 62, 62, 100-111.

APPENDIX 1. IRMAY'S EQUATION EXPRESSED IN FORCHHEIMER'S FORM

A1.1 INTRODUCTION

Numerous 1-D equations are available to predict V_i, the superficial fluid velocity required to initiate fluidization of a porous bed. However, in unbounded domains, the formation of both fluidized and unfluidized regions creates a more complicated problem. 2-D fluidization experiments reported by Roberts et al. (1986) provide a database of information on flow rates and hydraulic heads before and after incipient fluidization. The 1-D theoretical V_i compares favorably with the 2-D experimental data.

Many nonlinear equations are available to predict incipient fluidization. Irmay's equation predicts 2-D behavior adequately for many purposes if the key parameters are correctly determined. These key parameters include the porosity, sphericity, and equivalent grain diameter. The higher the sphericity (ψ), the less angular the grains and the lower the fixed bed porosity. Additional information on sphericity and other parameters are available in Cleasby and Fan (1981) and Fan (1978).

Many traditional applications of 1-D fluidization are

summarized in references such as Weisman et al. (1988). Intentional 1-D fluidization often results from a well-distributed source of upflowing fluid under a bed of solid particles confined by lateral boundaries. As fluid flows upward, head loss occurs through the bed as a result of viscous and inertial effects. The superficial velocity, V, is the upward volumetric flow rate divided by the total cross-sectional area of the fluidized domain. For Reynolds numbers, R, less than 3 the head loss through the fixed bed is a linear function of the flow rate, where $R = Vd_{eq}/\mu$, d_{eq} = grain diameter of a sphere of equal volume, μ = kinematic viscosity of water. Camp (1964) has reported strictly laminar flow through filters up to R = 6. The minimum V causing fluidization is V_i, occurring when the upward drag equals the submerged weight of the particles.

A1.2 EXPERIMENTAL DATA OF ROBERTS ET AL. (1986)

Weisman et al. (1988) summarize Roberts et al.'s (1986) experiments, with emphasis on the processes occurring after fluidization. Flow emanates from perforations in a source pipe buried in sand. Fine sand was chosen because it has the size, shape, and consistency of material found in the coastal environment. The sand has a specific gravity of 2.67, compacted porosity of 39%, d_{50} = 0.15 mm ,and d_{90} = 0.21 mm.

Because of the uniformity of the sand, estimates of K based on d_{50} will not differ too much from estimates based on other sizes. The sphericity was assumed to be 0.8. Only a slight bed expansion occurred prior to incipient fluidization. Based upon these values, K was estimated to be 0.0125 cm/s, in good agreement with the values obtained by Roberts et al. (1986). For low flow rates, the bed remains unfluidized. As the flow rate is slowly increased in discrete increments, a local boil on the sand surface occurs above the pipe. A slight increase in flow rate results in enlarged boils that coalesce until the bed above the supply pipe is fluidized along its entire length. The transition from an unfluidized to a completely fluidized bed is a rather unstable phenomena. If the flow rate is high enough, 2-D fluidization occurs as shown in Figure A.1.

Prior to incipient fluidization, almost half of the flow is into areas that won't fluidize even at much higher flow rates. Because of this "leakage", the flow rate required to initiate fluidization is expected to be greater than if the domain was bounded below and close to the sides of the source pipe.

Head data were obtained just prior to incipient fluidization, and were used to estimate incipient conditions, including the critical hydraulic gradient, i_c. For burial depths of 25.4 and 42 cm, i_c = 1.06 and 1.25, Q_i = 0.090 and 0.135 l/s-m, and V_i = 0.039 and 0.048 cm/s, respectively.

APPENDIX 2. USER'S MANUAL: FINITE ELEMENT ANALYSIS OF INCIPIENT FLUIDIZATION

USER'S MANUAL: FINITE ELEMENT ANALYSIS OF INCIPIENT FLUIDIZATION (PROGRAM FEF)

INTRODUCTION

A programmer's manual is presented for a finite element analysis package. The first program segment is a preprocessor that reads, prints, and scans the data, and generates required data. Data files are created which are used in the analysis (second) program segment which produces the required solution. Three types of finite elements may be used, 3-noded linear triangular elements, Q-8 elements, and 6-noded quadratic triangular elements. The third program segment for linear triangular elements includes a post processor to display the results. The program is coded in FORTRAN 77.

1. PREPROCESSOR: PROGRAM PREP

1.1 Introduction

To save effort in preparing input data for the analysis, the preprocessor provides options for data generation. The region to be analyzed should be sketched and coordinate axes defined. The location of the coordinate origin is arbitrary. The finite element region is divided into a mesh of elements with nodal points numbered in a numerical sequence starting with 1. In order to obtain a minimum bandwidth (which saves computation time when solving the system of equations), the nodal points should be numbered in the "shorter" direction, i.e. the one which has less elements. The overall goal is to minimize the maximum difference between any two node numbers in any element. A list of the required input is presented in the user's manual.

1.2 Description of Preprocessor Program (Program PREP)

The coefficients in the governing equation are read in as constant values or variables. The preprocessor generates missing data for both elements and nodes. The first element in a row of elements is defined by its node numbers. Subsequent elements in the row have node number incremented by a specified number, often 1.

If node locationss are spaced equally apart, only the first and last node's (x,y) coordinates are specified; the coordinates in between are generated by linear interpolation.

Sample input, output and generated file listings are available for the authors on IBM PC compatible disk files.

1.3 Preprocessor

Record Type 1 - An 80 character title (one record only)

Record Type 2 - Coefficients for Cases with lower order derivative terms

- AA,BB,CC - Constant values of coefficients A, B, and C in Eq. 1 (see Section 2.3)
- DD - Coefficient of h term in Eq. 1

Record Type 3 - (one record only)

- NORDER - Element type (only one type of element may be used in any grid).
  1 for 3-noded linear triangular element.
  2 for Q-8 (8-noded quadratic) element.
  3 for 6-noded quadratic triangular element.
- NELEMC - The number of elements for which nodal numbers will be supplied and used to generate nodal numbers for the remaining elements.
- NNPC - The number of nodal points at which coordinates will be supplied so that coordinates of the remaining nodes can be generated.
- NPSI - Number of nodes on the boundary of D. Set = 0 for NORDER = 1 or 3.
- NPCV - If Q-8 elements are used, some midside nodes may fall on curved sides and their coordinates must be supplied to implement the generation option. NPCV is the total number of midside nodes on curved sides.
- KK - Flag used to control supression of debug print statements.
- IWRITE - Flag directing creation of record-image output files and debug prints (Analysis Program).
  -1- write global stiffness matrices on file 2
  0- write global stiffness matrices on file 2
  0- write solution on printers
  .ne.0- write solution on file 3
- ICASE - Case being analyzed: Not used as of 1985. Set equal to 4 for consistency with past and future versions of program
- IP - Number of quadrature points per Q-8 element set equal to zero if NORDER .ne.2.
- NPIN - Number of nodes where h is to be specified. If IBC = -1, h at all boundary nodes are set equal to zero.
- IBC - Number of nodes for boundary condition for type $h_i = h_j$. Input appears in pairs, both node i and node j.

Record Type 4 - Boundary Definition (As many records as needed)

- NPSIA(I) - (I = 1, NPSI). The node numbers of the boundary points, in counterclockwise order. If NPSI = 0 (for NORDER = 1 or 3), Record Type 4 is omitted.

Record Type 5 - Boundary Condition, h specified (As many records as needed).

NPIN(I), PIN(I) - (I = 1, NPIN) Node number where h is specified and value of h, respectively. If NPIN = -1, Record Type 5 is omitted.

Record Type 6 - Boundary Condition, $h_i = h_j$. (As many records as needed).

NBC(I) - (I = 1, IBC) For the head gradient = 0 on boundary, reduced to $h_i = h_j$, where node i is on boundary, and node j is in inward normal direction, input occurs in pairs, node i first, then node j. Omit if IBC = 0.

Record Type 7 - Element definition (As many records as needed).

NOD(I,J) - Nodal numbers of I^{th} element in counterclockwise direction, J = 1, NPE, where NPE = 3 for linear triangles, NPE = 8 for Q-8 elements, NPE = 6 for quadratic triangles.

NMIS - Number of successive elements whose nodal numbers are not provided and hence are generated.

NINC - The numerical difference in nodal numbers between the first generated and the present element. Its value is set equal to zero if the generation is to take place in the shorter direction.

Record Type 8 - nodal Coordinate Data (As many records as needed).

I - The node number

X(I) - The x-coordinate of node I

Y(I) - The y-coordinate of node I

NPMIS - = 1 if there is at least one node omitted between the present and the succeeding nodal coordinate data record, and hence generation is to be used. Otherwise set equal to zero.

NINC - The numerical difference between the succeeding and present node number. Set equal to zero if the generation is to take place in the shorter direction.

Record Type 9 - Mid-side node records (Only if Q-8 elements used)

I - The mid-side node number

X(I) - The x-coordinate of node I

Y(I) - The y-coordinate of node I

Record Type 10- The nodal points (x,y) are defined by the records in in Record Type 8 or 9. Record type 10 consists of (x,y) points which may or may not correspond to a nodal point. Whenever a point (x,y) from Record Type 10 is found to coincide with a grid point (x,y) from Record Type 8 or 9, the values of A, B, and C on Record Type 10 supersede the values of A, B, and C on Record Type 8 or 9.

XE,YE - (x,y) coordinates of Record Type 10 points

AE,BE,CE - Coefficients A,B, and C in Eq. 1 at (x,y)

1.4 Preprocessor Output

The output file echos the input data, and generates the input data file to the analysis program (see next section). The general quantities in the output consist of:

TITLE - 80 character title
NOD(,J) - element definition data
X(I), Y(I), AA(I), BB(I), CC(I) - nodal data I = 1, NNP
NPSIA(I) - boundary node numbers
NHBW = NCOL - half-bandwidth

A preprocessor output file and generated file for Program FEF are available from the authors on an IBM PC compatible disk file.

2. ANALYSIS PROGRAM: PROGRAM FEF

2.1 Introduction

The entire input file, including Record Types 1 and 2, is created by the preprocessor output. If not constant, the values of A, B and C must be entered through Record Type 10 of the Preprocessor Input. The governing equation is:

$$K_{xx} \frac{\partial^2 h}{\partial x^2} + K_{yy} \frac{\partial^2 h}{\partial y^2} + A(x,y) \frac{\partial h}{\partial x} + B(x,y) \frac{\partial h}{\partial y} + C(x,y) + Dh + \sum_{i=1}^{n} P_i \, \delta(x-x_i, y-y_i) = 0 \quad (1)$$

where:

K_{xx}	=	hydraulic conductivity in the x-direction
K_{yy}	=	hydraulic conductivity in the y-direction
A,B,C	=	functional coefficients (currently equal to zero)
D	=	non-coefficient is used for solving Helmholtz-type problems, read in analysis program but not in preprocessor.
P_i	=	flowrate of an internal sinks located at node i (currently read in analysis program but not in preprocessor)

2.2 Method of Weighted Residuals

With ϕ representing h, the hydraulic head,

$$\int_D W\, L(\phi)\, dA = 0 \tag{1}$$

Using $\bar{\phi} = \{N\}\ \{\phi\}_e$ in each element (2)

$$W = \{N\} \text{ in each element} \tag{3}$$

Then interchange of integration & summation (assuming error to be small) is

$$\sum_{e=1}^{m} \int_{A_e} \{N\}\ L(\bar{\phi})\, dA = 0 \tag{4}$$

Using

$$L(\phi) = K_{xx} \frac{\partial^2 \phi}{\partial x^2} + K_{yy} \frac{\partial^2 \phi}{\partial y^2} + A(x,y) \frac{\partial \phi}{\partial x} + B(x,y) \frac{\partial \phi}{\partial y} + C(x,y) + D\phi + \sum_{i=1}^{n} P_i\, \delta(x-x_i,\, y-y_i) \tag{5}$$

in Eq. (4) yields

$$\sum_{e=1}^{m} \int_{A_e} \{N\} \left[K_{xx} \frac{\partial^2 \bar{\phi}}{\partial x^2} + K_{yy} \frac{\partial^2 \bar{\phi}}{\partial y^2} + A \frac{\partial \bar{\phi}}{\partial x} + B \frac{\partial \bar{\phi}}{\partial y} + D\bar{\phi}\right] dA + \int_{A_e} \{N\}\, [C]\, dA + \int_{A_e} \sum_{i=1}^{n} \{N\}\, P_i\, \delta(x-x_i, y-y_i)\, dA = 0 \tag{6}$$

Using theorem if K_{xx} and K_{yy} are constant in an element

$$\sum_{e=1}^{m} -K_{xx} \int_{A_e} \frac{\partial \{N\}}{\partial x} \frac{\partial \bar{\phi}}{\partial x}\, dA - K_{yy} \int_{A_e} \frac{\partial \{N\}}{\partial y} \frac{\partial \phi}{\partial y}\, dA + \oint_S \{N\}\left(K_{xx} \frac{\partial \phi}{\partial x} + K_{yy} \frac{\partial \phi}{\partial y}\right) d\ell + \int_{A_e} \left(\{N\} A \frac{\partial \phi}{\partial x} + \{N\}\, B \frac{\partial \bar{\phi}}{\partial y} + \{N\}\, D\bar{\phi}\right) dA + \int_{A_e} \{N\}\, [C]\, dA + \sum_{e=1}^{m} \int_{A_e} \sum_{i=1}^{n} P_i\, \delta(x-x_i, y-y_i)\, dA = 0 \tag{7}$$

Using $\bar{\phi} = \{N\}^T \{\phi\}_e$ yields (8)

$$[K]\ \{\phi\} = \{R\} \tag{9}$$

where

$$[K] = \sum_{e=1}^{m} [k]$$

$$[k] = \Bigg[\{ \int_{A_e} (-K_{xx} \frac{\partial\{N\}}{\partial x} \frac{\partial\{N\}^T}{\partial x}) dA + \int_{A_e} (-K_{yy} \frac{\partial\{N\}}{\partial y} \frac{\partial\{N\}^T}{\partial y}) dA + \int_{A_e} (\{N\}A \frac{\partial\{N\}^T}{\partial x} + \{N\} B \frac{\partial\{N\}^T}{\partial y}) dA + \int_{A_e} \{N\}D \{N\}^T \Bigg] \tag{10}$$

$$\{R\} = \sum_{e=1}^{m} \{r\} + \{S\}$$

$$\{S\} = \{- \oint_S \{N\} (K_{xx} \frac{\partial\phi}{\partial x} + K_{yy} \frac{\partial\phi}{\partial y}) d\ell$$

$$\{r\} = -\int_{A_e} \{N\} C\, dA$$

$$-\int_{A_e} \sum_{i=1}^{n} \{N\} P_i \delta(x-x_i, y-y_i) dA \tag{11}$$

2.3 Details of assembly

Now for K_{xx}, K_{yy}, and D constant in an element and expressing

$A = \{N\}^T\{A\}$, $B = \{N\}^T\{B\}$, $C = \{N\}^T\{C\}$ then Eq. 10 becomes

for linear triangular elements

$$[K] = \left[-K_{xx} \frac{\partial N_i}{\partial x} \frac{\partial N_i}{\partial x} \left[\int_{A_e} dA\right] - K_{yy} \frac{\partial N_i}{\partial y} \frac{\partial N_j}{\partial y} \left[\int_{A_e} dA\right]\right.$$

$$+ \int N_i \left(N_1A_1 + N_2A_2 + N_3A_3\right) \frac{\partial N_j}{\partial y} dA$$

$$+ \int N_i \left(N_1B_1 + N_2B_2 + N_3B_3\right) \frac{\partial N_j}{\partial y} dA$$

$$\left. + \int_{A_e} N_i \, D \, N_j \, dA\right] \tag{12}$$

Using the notation

$$N_i = \begin{Bmatrix} N_1 \\ N_2 \\ N_3 \end{Bmatrix} = \frac{1}{2A_e} \begin{Bmatrix} a_1 + b_1x + c_1y \\ a_2 + b_2x + c_2y \\ a_3 + b_3x + c_3y \end{Bmatrix} = \frac{1}{2A_e} \begin{Bmatrix} B_{11} + B_{21}x + B_{31}y \\ B_{12} + B_{22}x + B_{32}y \\ B_{13} + B_{23}x + B_{33}y \end{Bmatrix} \tag{13}$$

$$\int_{A_e} dA = A_e \tag{14}$$

$$BT_{i2} = B_{2i} = \begin{Bmatrix} \partial N_1/\partial x \\ \partial N_2/\partial x \\ \partial N_3/\partial x \end{Bmatrix} = \begin{Bmatrix} B_{21} \\ B_{22} \\ B_{23} \end{Bmatrix} \tag{15}$$

$$BT_{i3} = B_{3i} = \begin{Bmatrix} \partial N_1/\partial y \\ \partial N_2/\partial y \\ \partial N_3/\partial y \end{Bmatrix} = \begin{Bmatrix} B_{31} \\ B_{32} \\ B_{33} \end{Bmatrix} \tag{16}$$

Then

$$k_{ij} = K_{xx} \frac{\partial N_i}{\partial x} \frac{\partial N_j}{\partial x} A_e \quad -K_{yy} \frac{\partial N_i}{\partial x} \frac{\partial N_j}{\partial x} A_e$$

$$+ \{A_1 [\int_{A_e} N_1 N_i dA] + A_2 [\int_{A_e} N_2 N_i dA] + A_3 [\int_{A_e} N_3 N_i dA]\} \frac{\partial N_j}{\partial x}$$

$$+ \{B_1 [\int_{A_e} N_1 N_i dA] + B_2 [\int_{A_e} N_1 N_i dA] + B_3 [\int_{A_e} N_3 N_i dA]\} \frac{\partial N_j}{\partial y}$$

$$+ D \int_{A_e} N_i N_j \, dA \qquad (17)$$

2.4 The Dϕ term

Looking only at the Dϕ term entry to k_{ij}

$$k_{ij} \leftarrow D \int_{A_e} N_i N_j \, dA = D \begin{bmatrix} \int N_1 N_1 \, dA & \int N_1 N_2 \, dA & \int N_1 N_3 \, dA \\ \int N_2 N_1 \, dA & \int N_2 N_2 \, dA & \int N_2 N_3 \, dA \\ \int N_3 N_1 \, dA & \int N_3 N_2 \, dA & \int N_3 N_3 \, dA \end{bmatrix}$$

$$= \frac{D}{2A_e} \begin{bmatrix} Al_{11} & Al_{12} & Al_{13} \\ Al_{21} & Al_{22} & Al_{23} \\ Al_{31} & Al_{32} & Al_{33} \end{bmatrix}$$

$$D \int_{A_e} N_i N_j \, dA = D \begin{bmatrix} \int N_1 N_1 \, dA & \int N_1 N_2 \, dA & \int N_1 N_3 \, dA \\ \int N_2 N_1 \, dA & \int N_2 N_2 \, dA & \int N_2 N_3 \, dA \\ \int N_3 N_1 \, dA & \int N_3 N_2 \, dA & \int N_3 N_3 \, dA \end{bmatrix}$$

Proceed term by term $i,j = 1,2$ or 3

$$D \int N_i N_j \, dA = D \int \left[\frac{a_i + b_i x + c_i y}{2A^e} \quad \frac{a_j + b_j x + c_j y}{2A^e} \right] dA$$

$$= \frac{D}{4A_e^2} \left[a_i \int (a_j + b_j x + c_j y) \, dA + b_i \int (a_j + b_j x + c_j y) \, x \, dA \right.$$

$$\left. + c_i \int (a_j + b_j x + c_j y) \, y \, dA \right]$$

$$= \frac{D}{4A_e^2} \Big[\textcircled{a_i} \left(\textcircled{a_j} \textcircled{A_e} \; B_{i1}^T B_{j1}^T A7_{11} + \textcircled{b_j} \textcircled{\bar{x} A_e} \; B_{j2}^T A7_{12} + \textcircled{c_j} \textcircled{\bar{y} A_e} \; B_{j3}^T A7_{13} \right)$$

$$+ \textcircled{b_i} \left(\textcircled{a_j} \textcircled{\bar{x} A_e} \; B_{i2}^T B_{j1}^T A7_{21} + \textcircled{b_j} \textcircled{\bar{x}^2 A_e} \; B_{j2}^T A7_{22} + \textcircled{c_j} \textcircled{\bar{x}\,\bar{y} A_e} \; B_{j3}^T A7_{23} \right)$$

$$+ \textcircled{c_i} \left(\textcircled{a_j} \textcircled{\bar{y} A_e} \; B_{i3}^T B_{j1}^T A7_{31} + \textcircled{b_j} \textcircled{\bar{x}\,\bar{y} A_e} \; B_{j2}^T A7_{32} + \textcircled{c_j} \textcircled{\bar{y}^2 A_e} \; B_{j3}^T A7_{33} \right) \Big]$$

Redefining each circled quantity by the quantity in the hexagon below it results in:

$$= \frac{D}{4A_e^2} \left[B_{i1}^T \left(B_{j1}^T A7_{11} + B_{j2}^T A7_{12} + B_{j3}^T A7_{13} \right) \right.$$

$$+ B_{i2}^T \left(B_{j1}^T A7_{21} + B_{j2}^T A7_{22} + B_{j3}^T A7_{23} \right)$$

$$\left. + B_{i3}^T \left(B_{j1}^T A7_{31} + B_{j2}^T A7_{32} + B_{j3}^T A7_{33} \right) \right]$$

By definition $A7_{ij} = A7_{ji}$

$$Al_{jm} = \frac{B_{jk}^T A7_{km}}{2A_e} = \left(B_{j1}^T A7_{1m} + B_{j2}^T A7_{2m} + B_{j3}^T A7_{3m} \right) / 2A_e$$

So previous line can be written as

$$= \frac{D}{2Ae} \left[B_{1i} \left(Al_{j1} \right) + B_{2i} \left(Al_{j2} \right) + B_{3i} \left(Al_{j3} \right) \right]$$

$$= \frac{D}{2Ae} \left[B_{mi} \, Al_{jm} \right] = \frac{D}{2Ae} \left(Al_{jm} \, B_{mi} \right)$$

2.5 The C(x,y) term

$$\int N_i \, C(x,y) dA$$

$$= \int N_i \, N_j \, C_j \, dA$$

$$= C_1 \int N_i \, N_1 \, dA + C_2 \int N_i \, N_2 \, dA + C_3 \int N_i \, N_3 \, dA$$

2.6 Sample Problem - 1 element

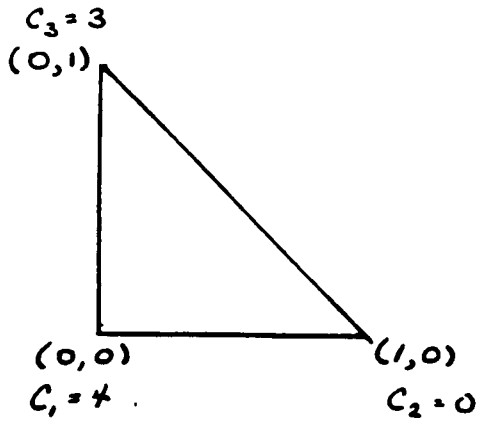

$x_i = 0 \qquad y_i = 0$

$x_j = 1 \qquad y_j = 0$

$x_k = 0 \qquad y_k = 1$

$A = \frac{1}{2} \{0 + 1\ (1-0) + 0\} = \frac{1}{2}$

$B_{11} = x_j\ x_k - y_j\ x_k = (1)\ (1) - 0 \cdot 0 = 1$

$B_{12} = x_k\ y_i - y_k\ x_i = 0$

$B_{13} = x_i y_j - y_i x_j = 0$

$B_{21} = -1$

$B_{22} = 1$

$B_{23} = 0$

$B_{31} = -1$

$B_{32} = 0$

$B_{33} = 1$

$C_1^i = B_{11}\ C_1^e + B_{12}\ C_2^e + B_{13}\ C_3^e$

$= (1)(4) + (0)(0) + (0)(3) = 3$

$C_2^i = B_{21}\ C_1^e + B_{22}\ C_2^e + B_{23}\ C_3^e$

$= (-1)(4) + (1)(0) + (0)(3) = -3$

$C_3^i = B_{31} C_1^e + B_{32}\ C_2^e + B_{33}^e\ C_3^e$

$= (-1)(4) + (1)(0) + (1)(3) = 0$

2.7 Analysis Input

Record Type 1 - An 80-character field for titles on input, output, and files (one record only).

Record Type 2 - Coefficients and scaling factors (one record only) as of July 1983, XSCALE, YSCALE, TXX, TYY are entered interactively.

- XSCALE - Scaling factor for x coordinates
- YSCALE - Scaling factor for y coordinates
- TXX,TYY,DD - Coefficients K_{xx}, K_{yy}, and D in Eq. 1. If any of these are varibles (different values for elements), enter - 99999 for that quantity.

Record Type 3 - (one Record only)

- NELEM - Total number of elements
- NNP - Total number of nodes
- NCOL - (number of upper codiagonals) + 1 (also equal to half bandwidth, NBHW)
- NPSI - Number of nodes on boundary
- NPIN - Number of nodes where h is specified
- IBC - Number of nodes for boundary conditions of the type $h_i = h_j$. Input appears in pairs, both node i and node j.
- KK - Flag used to control supression of debug print statements.
- IWRITE - Flag for directing creation of 80-character record (see Preprocessor Input)
- ICASE - Case being analyzed (see Preprocessor Input)
- NORDER - Type of element being analyzed (see Preprocessor Input)
- IP - Number of quadrature points per Q-8 elements. Set equal to zero if NORDER .ne. 2.

Record Type 4 - Boundary Definition (As many records as needed)

- NPSIA(I) - (i = 1, npsi). The node numbers of the boundary points, in counterclockwise order. Enter only if Q-8 elements are used (NORDER = 2).

Record Type 5 - Boundary Condition, h specified (As many records as needed).

- NPINA(I), PIN(I) - (I = 1, NPIN) Node number where h is specified, and value of h, respectively. Do not enter if NPIN = 0.

Record Type 6 - Boundary Condition, $h_i = h_j$ (As many records as needed).

- NBC(I) - (I = 1, IBC) For condition $h_i = h_j$, where node i is on the boundary, and node j is at any location; input occurs in pairs, node i first then node j. Do not enter if IBC = 0.

Record Type 7 - Element data for NELEM element (As many records as needed).

- NOD(I,J) - nodal numbers of I^{th} element in counterclockwise direction, J = 1, NPE, where NPE = 3 for linear triangles, NPE = 8 for Q-8 elements, NPE = 6 for

Record Type 8 - nodal Coordinate Data for NNP nodes (As many records as needed)

X(I)	-	The x-coordinate of node I
Y(I)	-	The y-coordinate of node I
AA(I)	-	Coefficient (A in Eq. 1)
BB(I)	-	Coefficient (B in Eq. 1)
CC(I)	-	Forcing function term (C in Eq. 1) at X(I), Y(I).

Record Type 9 - TXX, TYY, and DD Data (As many records as needed).

TXX(I),I=1, NELEM	-	If TXX = -99,999 enter values of K_{xx} in Eq. 1 for each element.
TYY(I),I=1, NELEM	-	If TYY = -99,999 enter values of K_{yy} in Eq. 1 for each element.
DD(I),I=1, NELEM	-	If D = -99,999 enter values of D in Eq. 1 for each element.

Record Type 10 - Scaling Factor for Pumpage. One record

FACDEL	-	Scaling Factor for P_i in Eq. 1. For pumping wells, FACDEL = -1; currently Record types 10 and 11 are not read, but can be reactivated within Program FEF.

Record Type 11 - Pumping Wells. One record for each well.

IDEL	-	Node number where node is located
QPUMP	-	Pumping rate of well, (P_i in Eq. 1)

2.8 Analysis Output

Output - The main output includes: the element definition data (if IWRITE $\geq$ 0); the nodal coordinates (x,y), the solution h at the node and the partial derivatives of h, (if IWRITE = 0).

Files - File 2: Global stiffness matrix if IWRITE = -1, and element stiffness matrices (if IWRITE = 0).
File 3: Solution is written on file 3 if IWRITE .ne. 0 (solution is not printed).

Example output files are available from the authors on IBM PC compatible disks.

3. POST PROCESSOR

The post-processor interpolates the pressure field within an element using a linear interpolation scheme. If a contour passes through an element, a straight line segment from (x_1, y_1) to (x_2, y_2) will occur. Figure 1 shows such a contour line for h = 10 passes through an element with $h_i = 7$, $h_j = 5$, and $h_k = 13.5$.

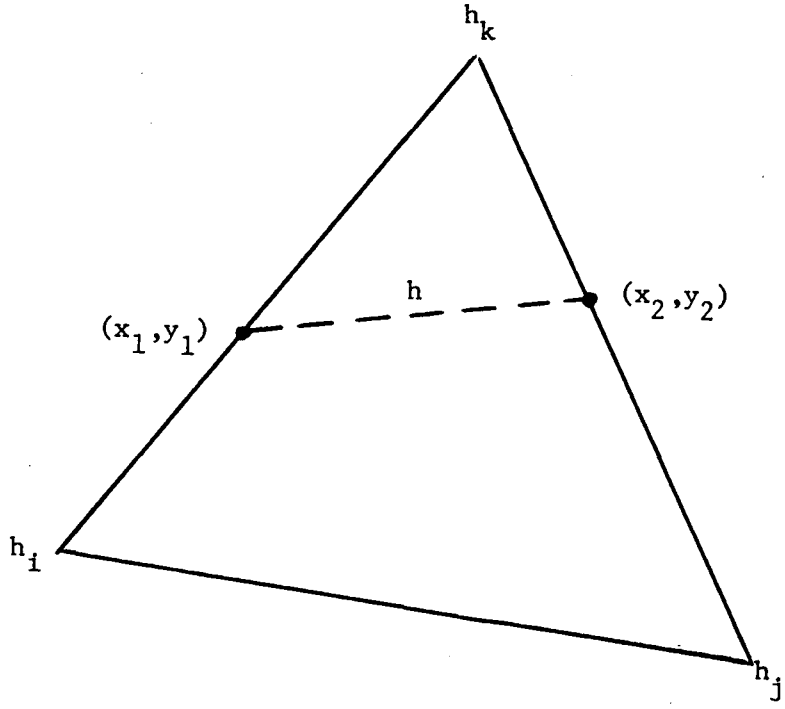

$h < h_k$

$h > h_i$

$h > h_j$

Figure 1.

APPENDIX 5. NOTATION

The following symbols are used in this paper:

a = coefficient in Irmay's (1958) Equation

A = coefficient in Forchheimer's Equation

b = coefficient in Irmay's (1958) Equation

B = coefficient in Forchheimer's Equation

d = equivalent sand grain diameter (mm)

D = diameter of fluidization source pipe (m)

d_b = depth of burial of fluidization source pipe

d_{50} = equivalent sand grain diameter exceeded by 50% of sand grains (by weight) (mm)

d_{90} = equivalent sand grain diameter exceeded by 90% of sand grains (by weight) (mm)

g = gravitational acceleration (9.81 m/s)

K = hydraulic conductivity (cm/s)

K_x = hydraulic conductivity in x (horizontal) direction (cm/s)

K_y = hydraulic conductivity in y (vertical) direction (cm/s)

n = porosity of porous medium

Q_i = minimum fluidization flow rate per unit width (cc/s/cm or l/s-m)

R = Reynolds number

R_v = ratio of inertia term to Darcy term in Eq. 2

V or q = Specific discharge; also superficial velocity for one-dimensional problems and Darcy velocity if Darcy's Law is valid (cm/s)

V_i = Minimum fluidization superficial velocity (cm/s)

μ = kinematic viscosity of water (g/cm/s)

ρ = fluid density (g/cc)

ρ_s = density of porous medium (g/cc)

ψ = sphericity of sand grains

X_b = horizontal (x) distance to impermeable side boundaries

Y_b = vertical distance from the centerline of the source pipe to the impermeable boundary below the source pipe

Table 2.1. Variation of gradient above source pipe for Roberts et al.'s (1986) incipient fluidization condition, 42 cm bed.

Measuring Location	Head at measuring Location, cm	Elevation Interval Between Measuring Location, cm	Average Gradient Between Measuring Location, cm
Top of Sand	0		
		32.1 to 42	0.87
Tap 74	3.38		
		24.5 to 32.1	0.93
Tap 59	6.17		
		16.8 to 24.5	0.93
Tap 44	8.96		
		9.2 to 16.8	1.21
Tap 29	12.6		
		1.6 to 9.2	1.64
Tap 14	17.5		
		0 to 1.6	-
Pipe	-		
Weighted Average			1.10

" - " indicates data not available.

Table 3.1. Variation of h_{max}/d_b for the simulated conditions.

	Isotropic		K_x/K_y = 10:1	
Depth, ft	Small Domain*	Large Domain**	Small Domain*	Large Domain**
5	2.47	2.50	2.16	2.24
10	2.20	2.26	1.91	2.09
20	1.96	2.06	1.62	1.95
40	1.69	1.87	1.37	1.80

* X_d = 50 ft, Y_d = 20 ft.

** X_d = 3000 ft. Y_d = 240 ft.

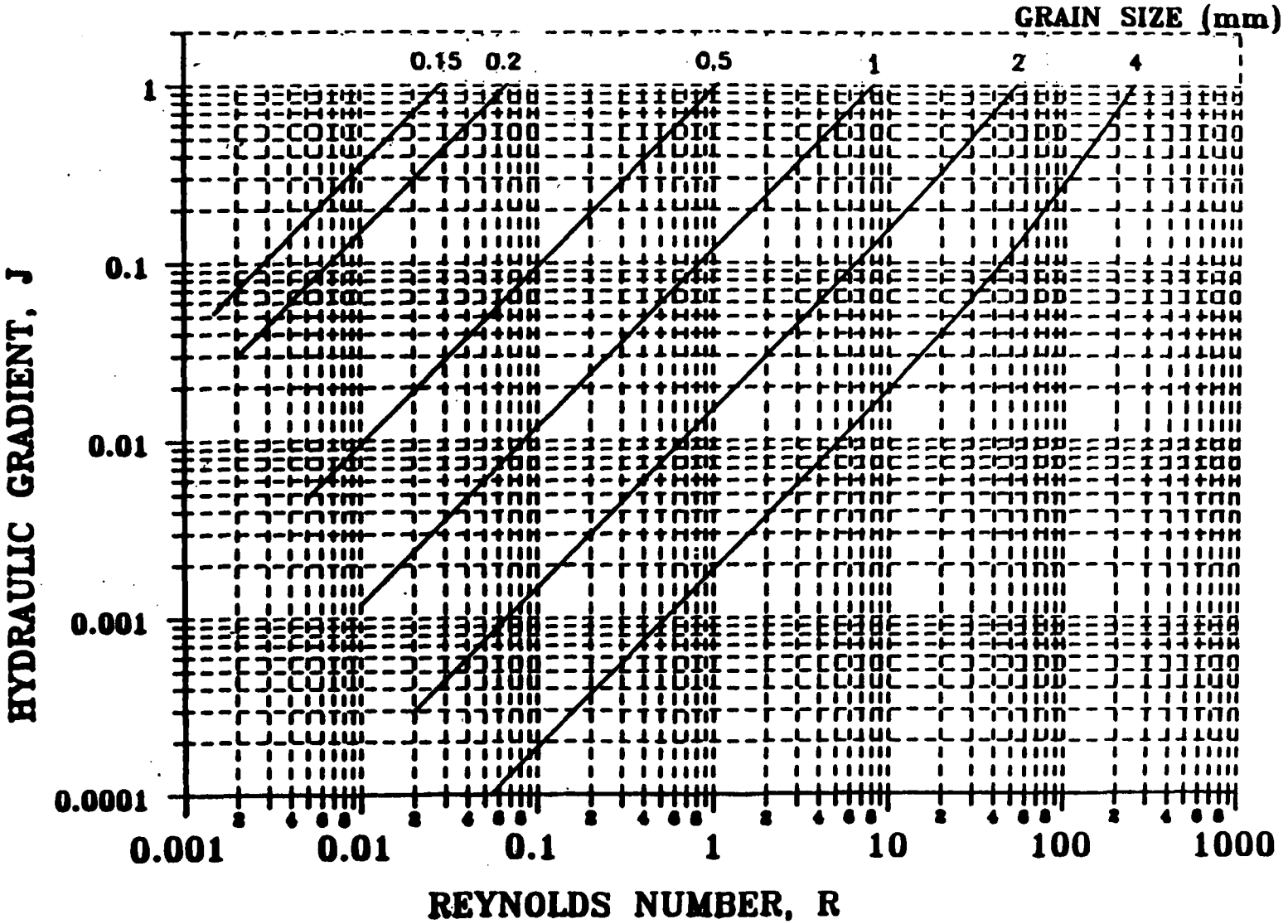

Figure 2.1 Predicted hydraulic gradient versus Reynolds Number using Irmay's (1958) equation.

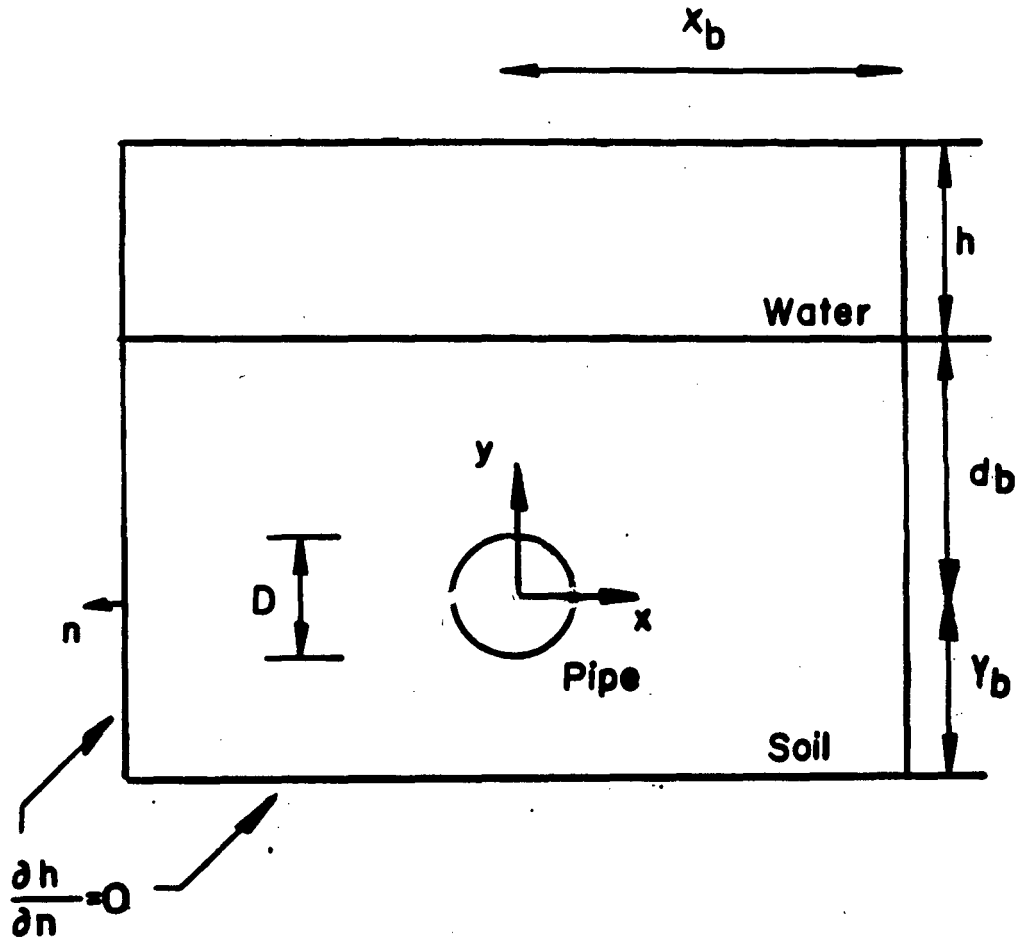

Figure 2.2 Definition sketch of a source pipe buried a depth d_b in a fine sand prior to incipient fluidization.

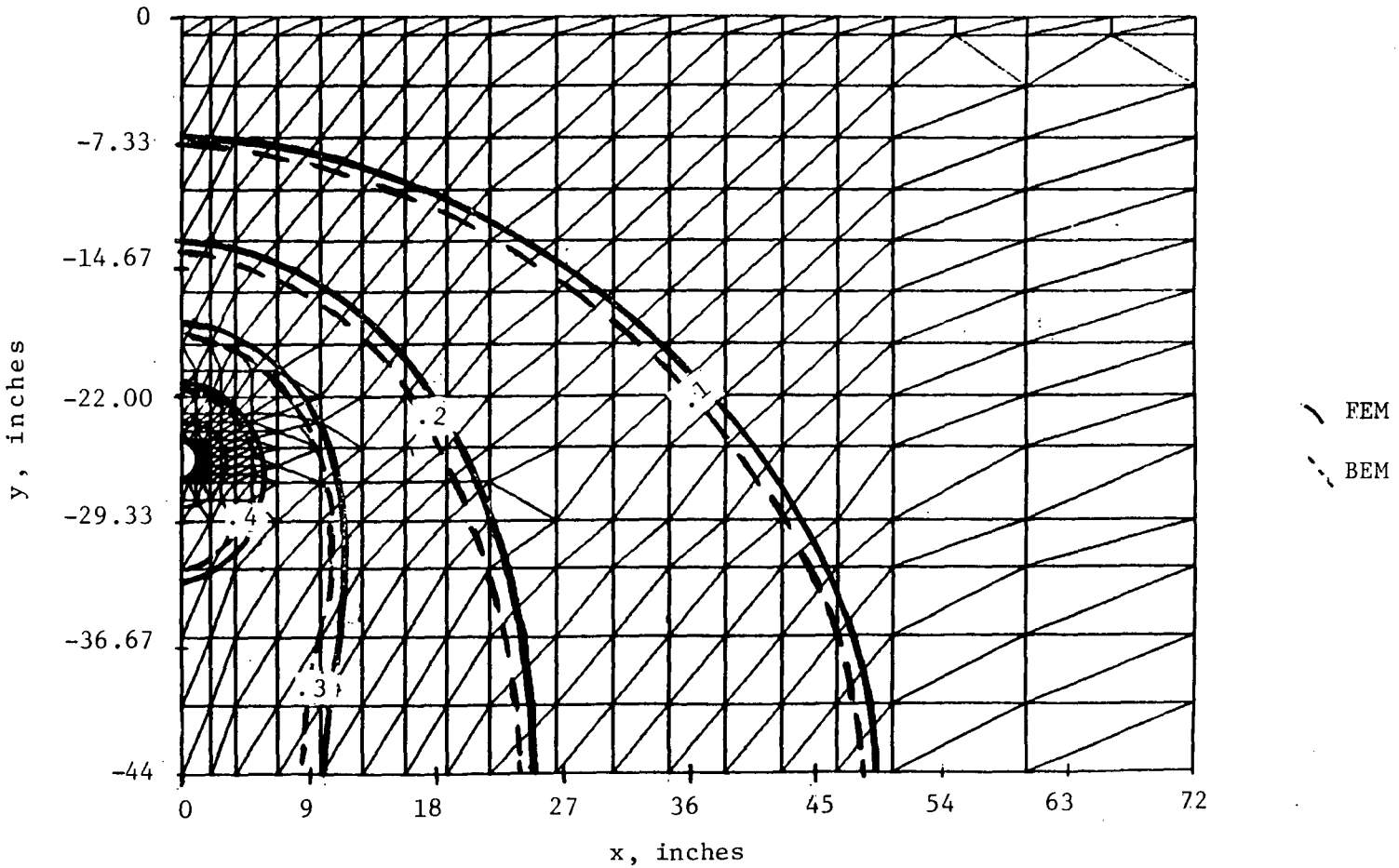

Figure 3.1 Comparison of finite element and boundary element results for a hypothetical problem of a 26 inch burial depth; contours are fraction of maximum value.

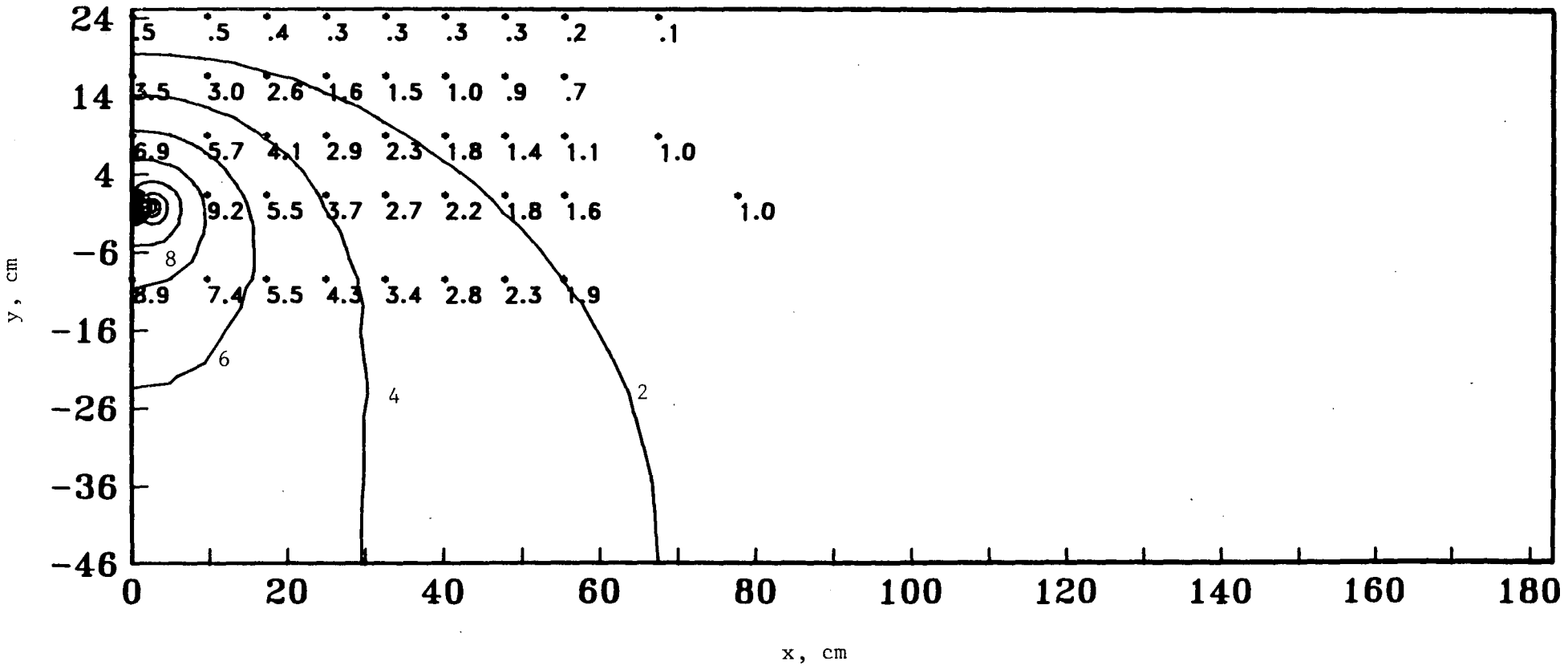

Figure 3.2 Comparison of Roberts et al.'s (1986) Test 2 observed head data (to tenths of cm) with predicted contours of hydraulic head (cm) using the finite element method for a flow rate of 0.0344 l/s-m, K_x = 0.012 cm/s, K_y = 0.012 cm/s.

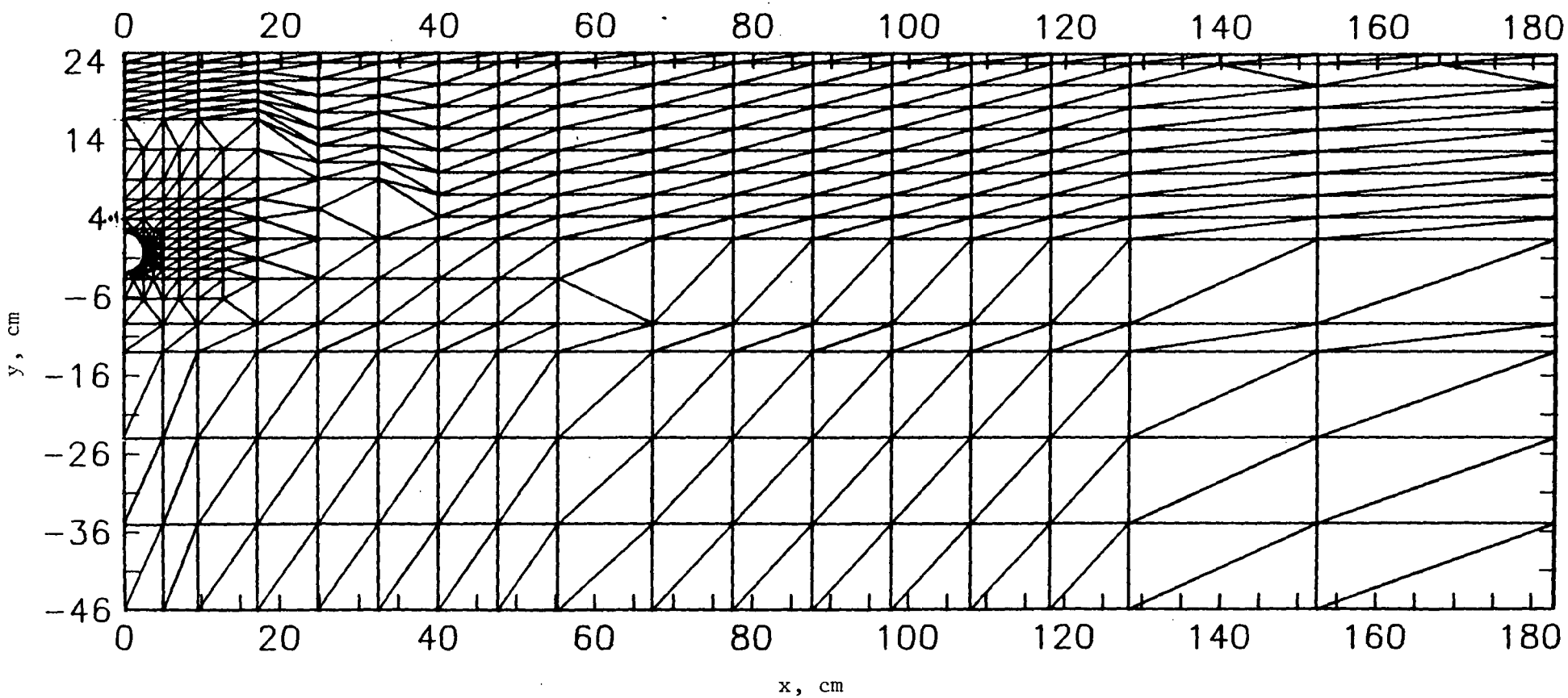

Figure 3.3 Computational finite element grid used in the calculation of numerical results for verification with Roberts et al. (1986) data using 715 elements and 404 nodes.

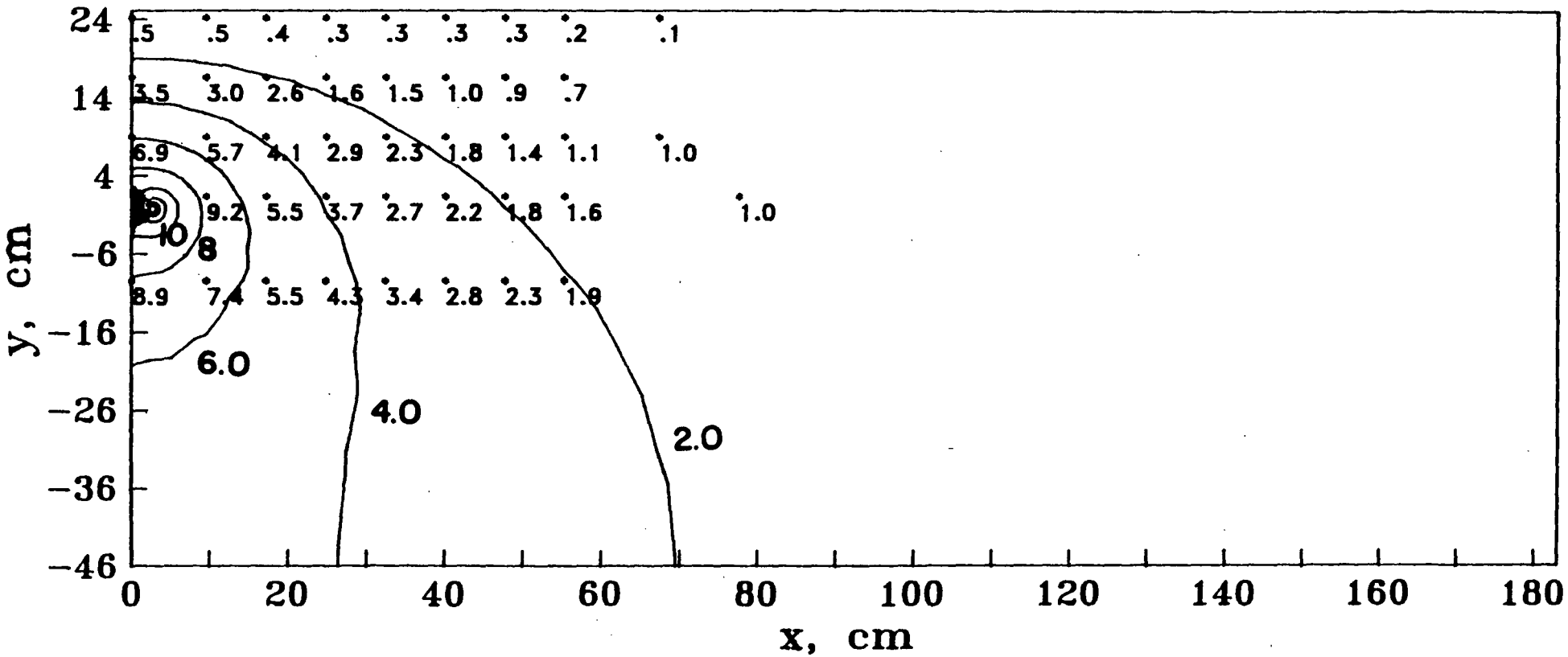

Figure 3.4 Comparison of Roberts et al.'s (1986) Test 2 observed head data (to tenths of cm) with predicted contours of hydraulic head (cm) using the finite element method for a flow rate of 0.0344 l/s-m, K_x = 0.014 cm/s, K_y = 0.012 cm/s.

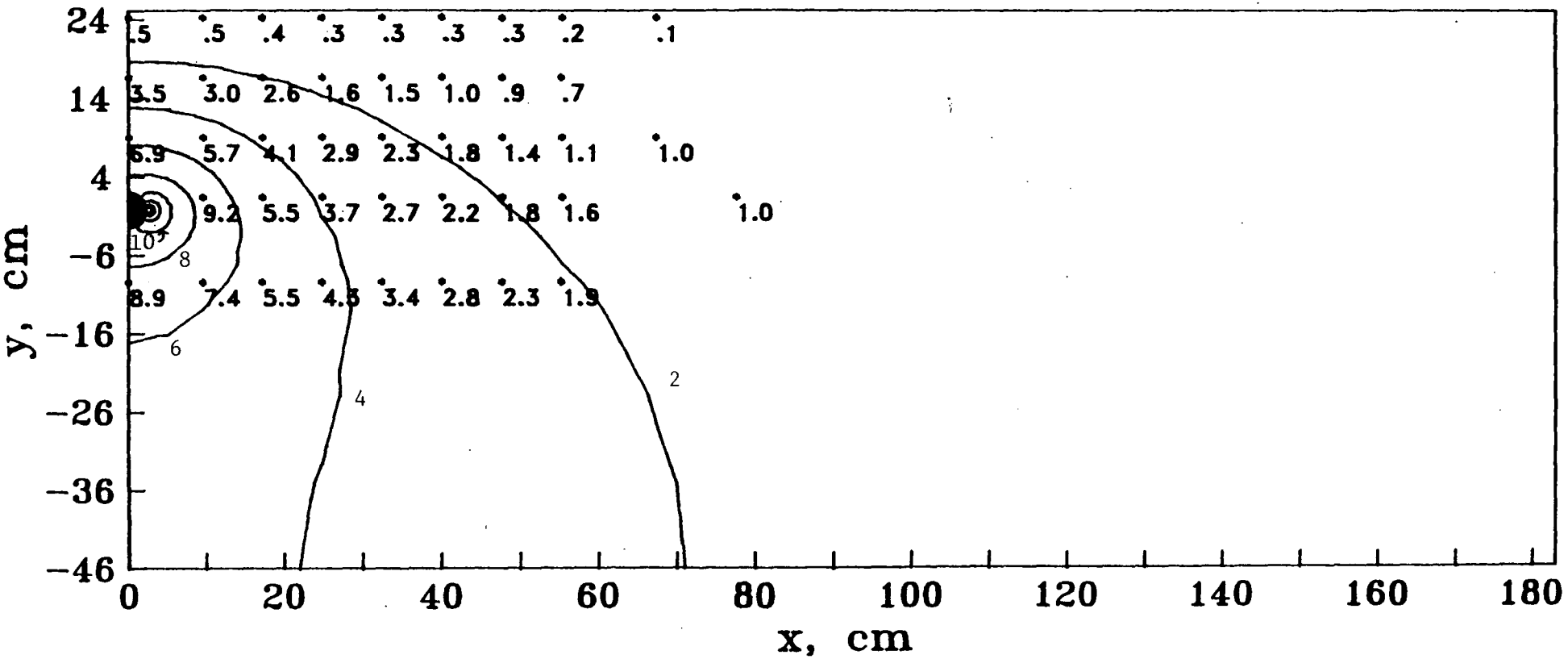

Figure 3.5 Comparison of Roberts et al.'s (1986) Test 2 observed head data (to tenths of cm) with predicted contours of hydraulic head (cm) using the finite element method for a flow rate of 0.0344 l/s-m, K_x = 0.016 cm/s, K_y = 0.012 cm/s.

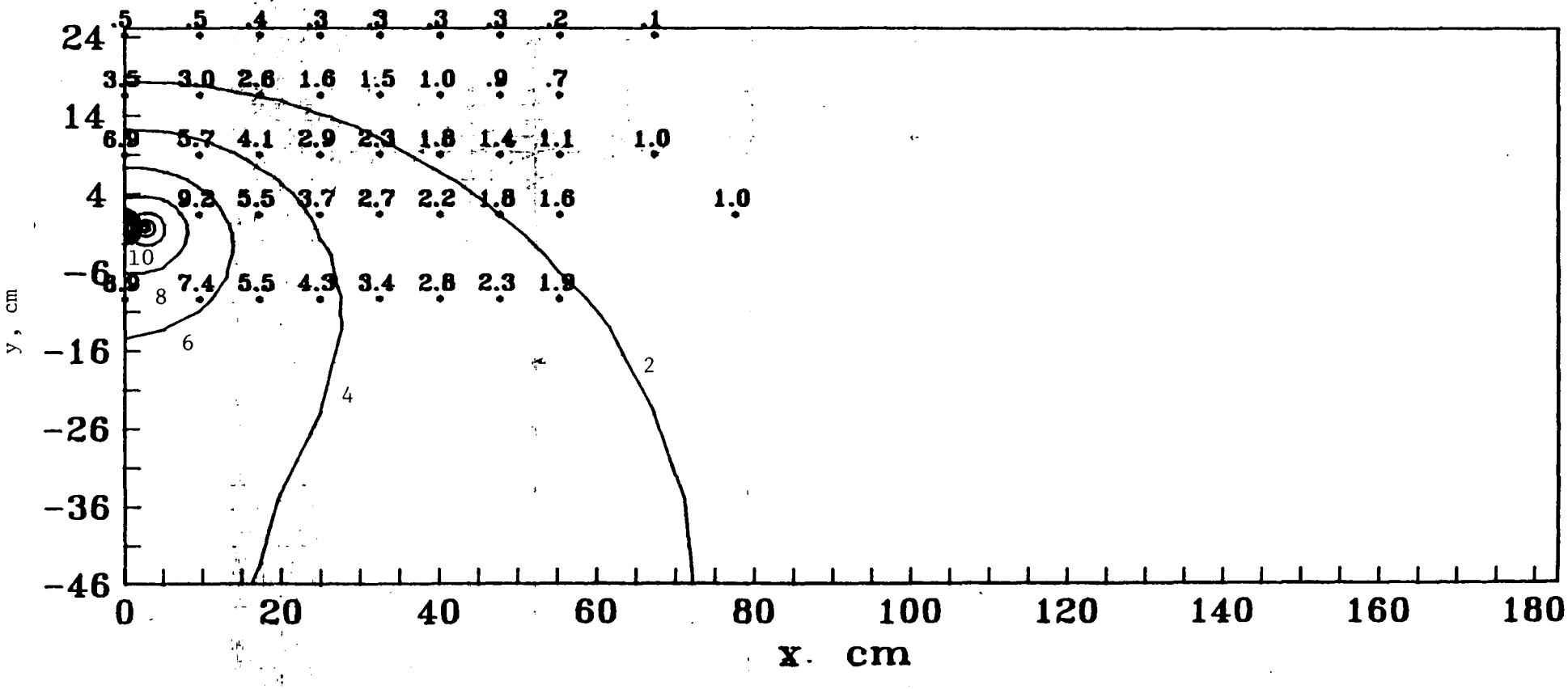

Figure 3.6 Comparison of Roberts et al.'s (1986) Test 2 observed head data (to tenths of cm) with predicted contours of hydraulic head (cm) using the finite element method for a flow rate of 0.0344 l/s-m, K_x = 0.018 cm/s, K_y = 0.012 cm/s.

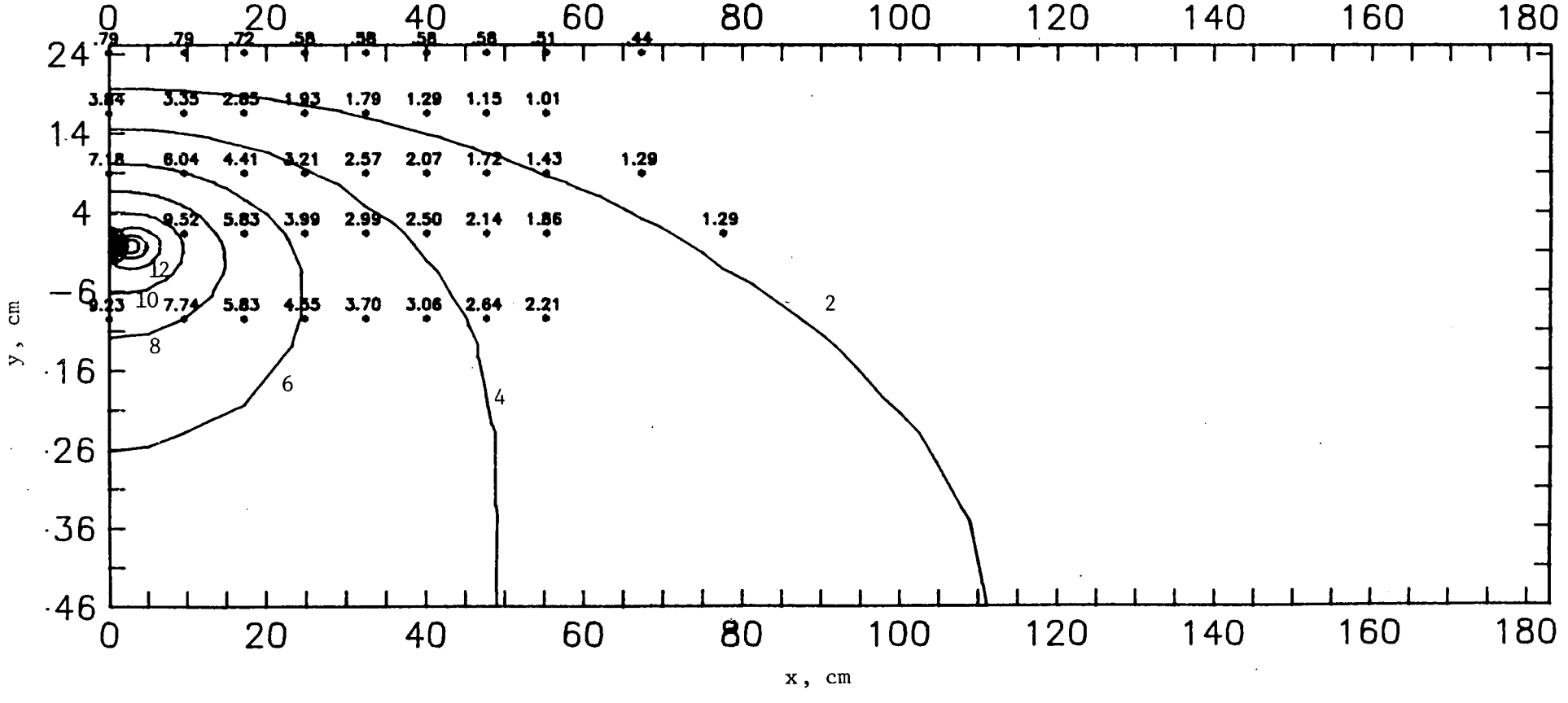

Figure 3.7 Comparison of Roberts et al.'s (1986) Test 2 observed head data (to hundredths of cm) with predicted contours of hydraulic head (cm) using the finite element method for a flow rate of 0.0344 l/s-m, K_x = 0.018 cm/s, K_y = 0.008 cm/s.

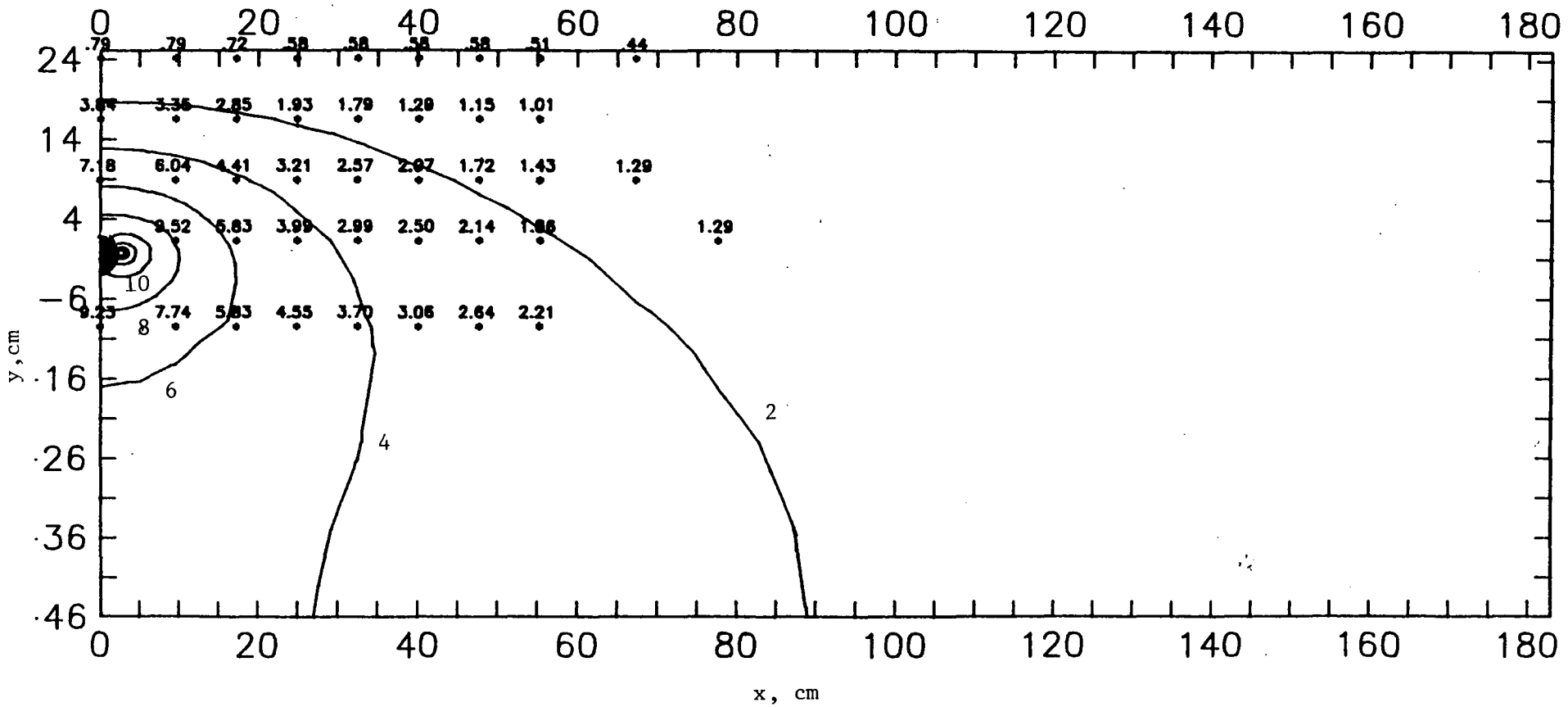

Figure 3.8 Comparison of Roberts et al.'s (1986) Test 2 observed head data (to hundredths of cm) with predicted contours of hydraulic head (cm) using the finite element method for a flow rate of 10.45 cc/s (0.0344 l/s-m), K_x = 0.02 cm/s, K_y = 0.01 cm/s.

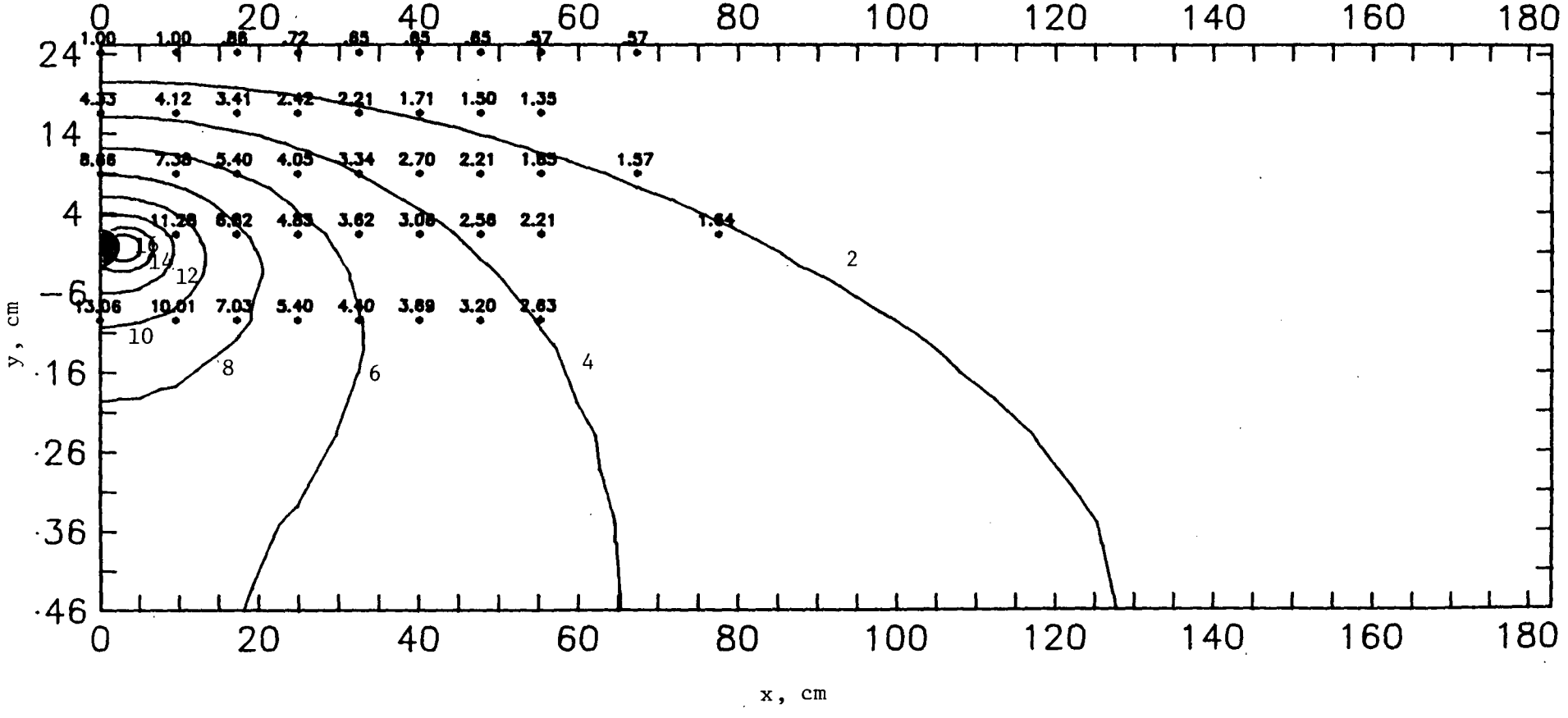

Figure 3.9 Comparison of Roberts et al.'s (1986) Test 2 observed head data (to hundredths of cm) with predicted contours of hydraulic head (cm) using the finite element method for a flow rate of 12.47 cc/s, K_x = 0.018 cm/s, K_y = 0.008 cm/s.

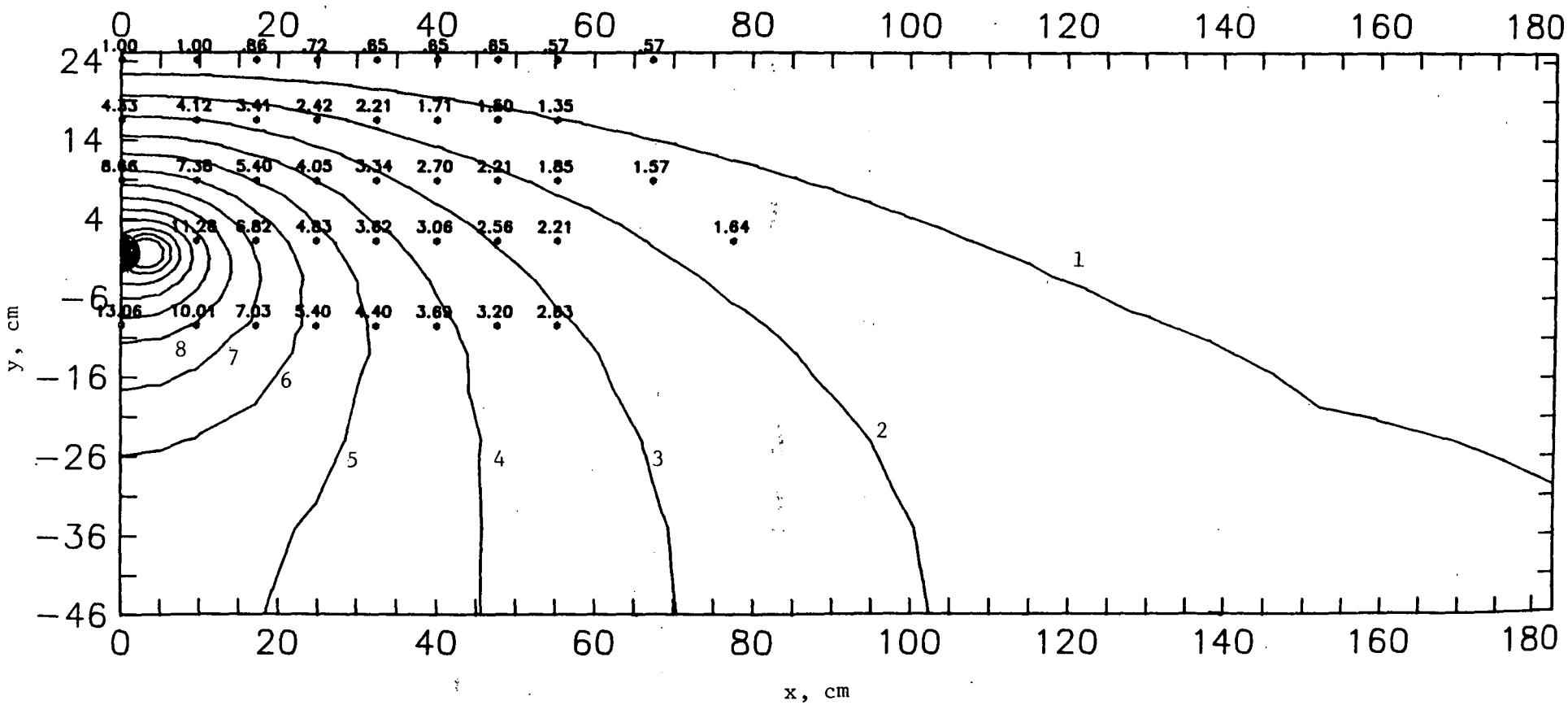

Figure 3.10 Comparison of Roberts et al.'s (1986) Test 2 observed head data (to hundredths of cm) with predicted contours of hydraulic head (cm) using the finite element method for a flow rate of 12.47 cc/s, K_x = 0.02 cm/s, K_y = 0.008 cm/s.

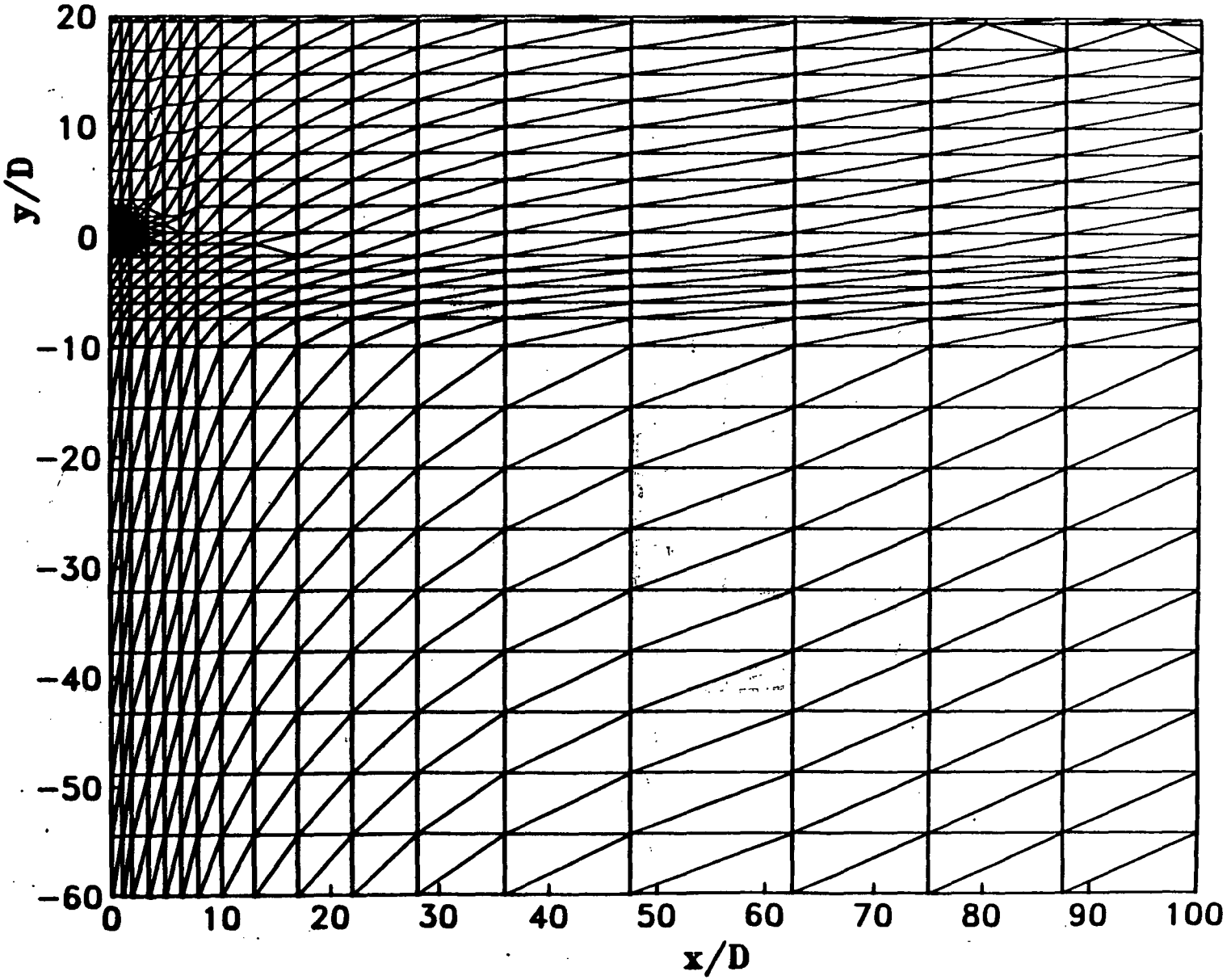

Figure 3.11 Computational finite element grid used in the calculation of numerical results for design chart using 1055 elements and 584 nodes.

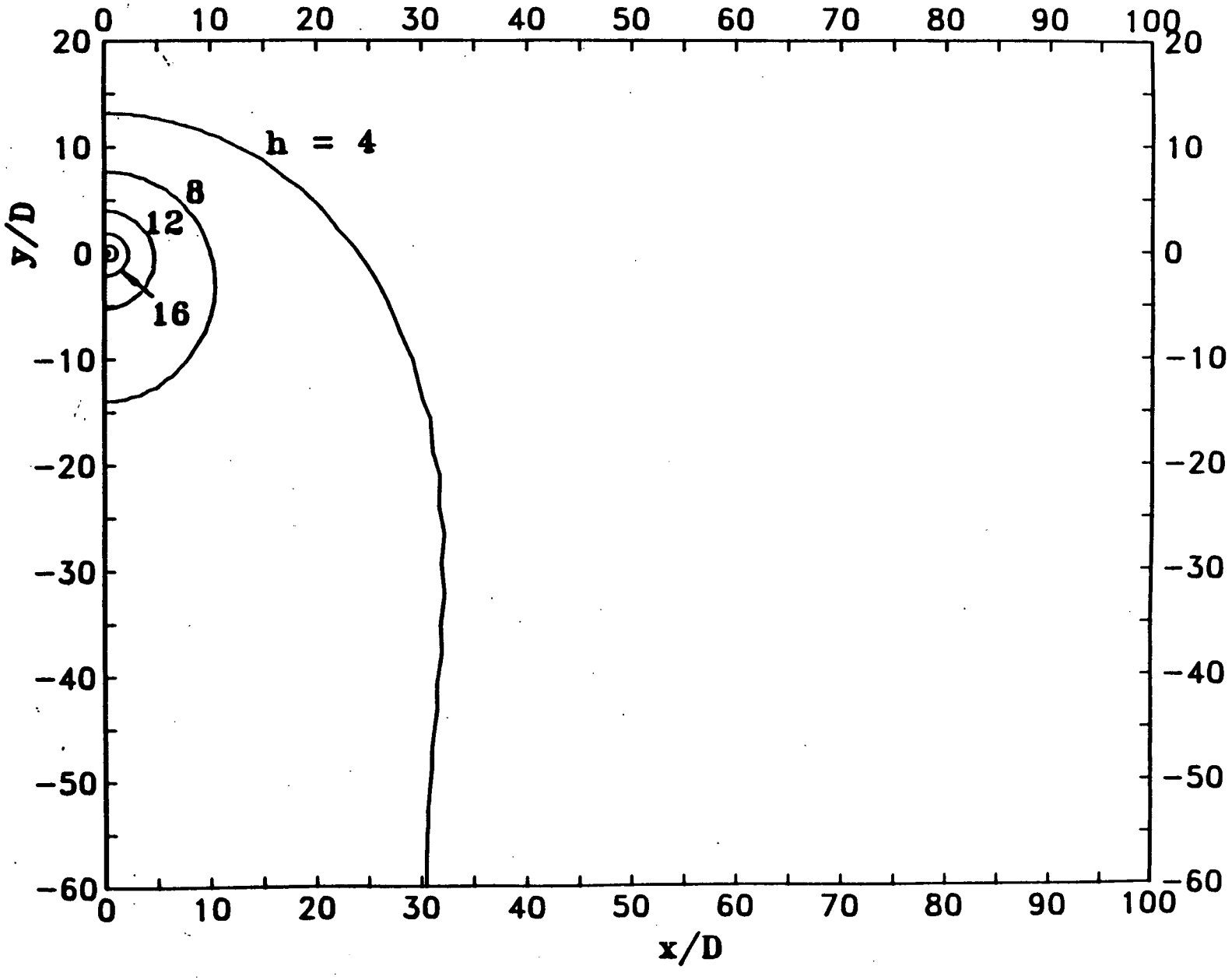

Figure 3.12 Predicted hydraulic head contours for a 1 ft (0.305 m) diameter pipe buried 20 ft (6.10 m) in a domain with X_d = 100 ft (30.5 m) and Y_d = 60 ft (18.3 m).

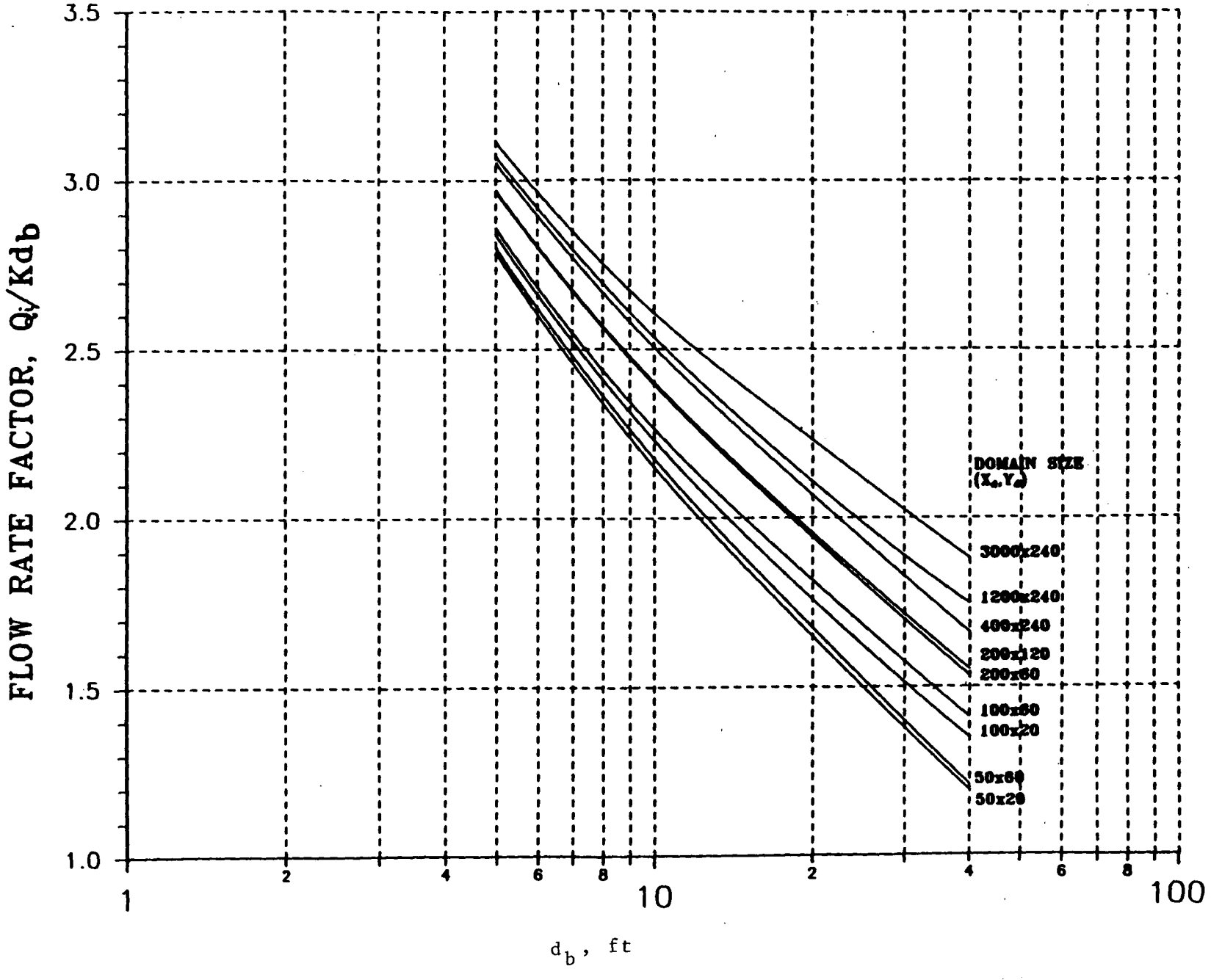

Figure 3.13a Design chart for isotropic conditions providing the required flow rate factor (Q_i/Kd_b) versus depth of burial, d_b, for various domain sizes.

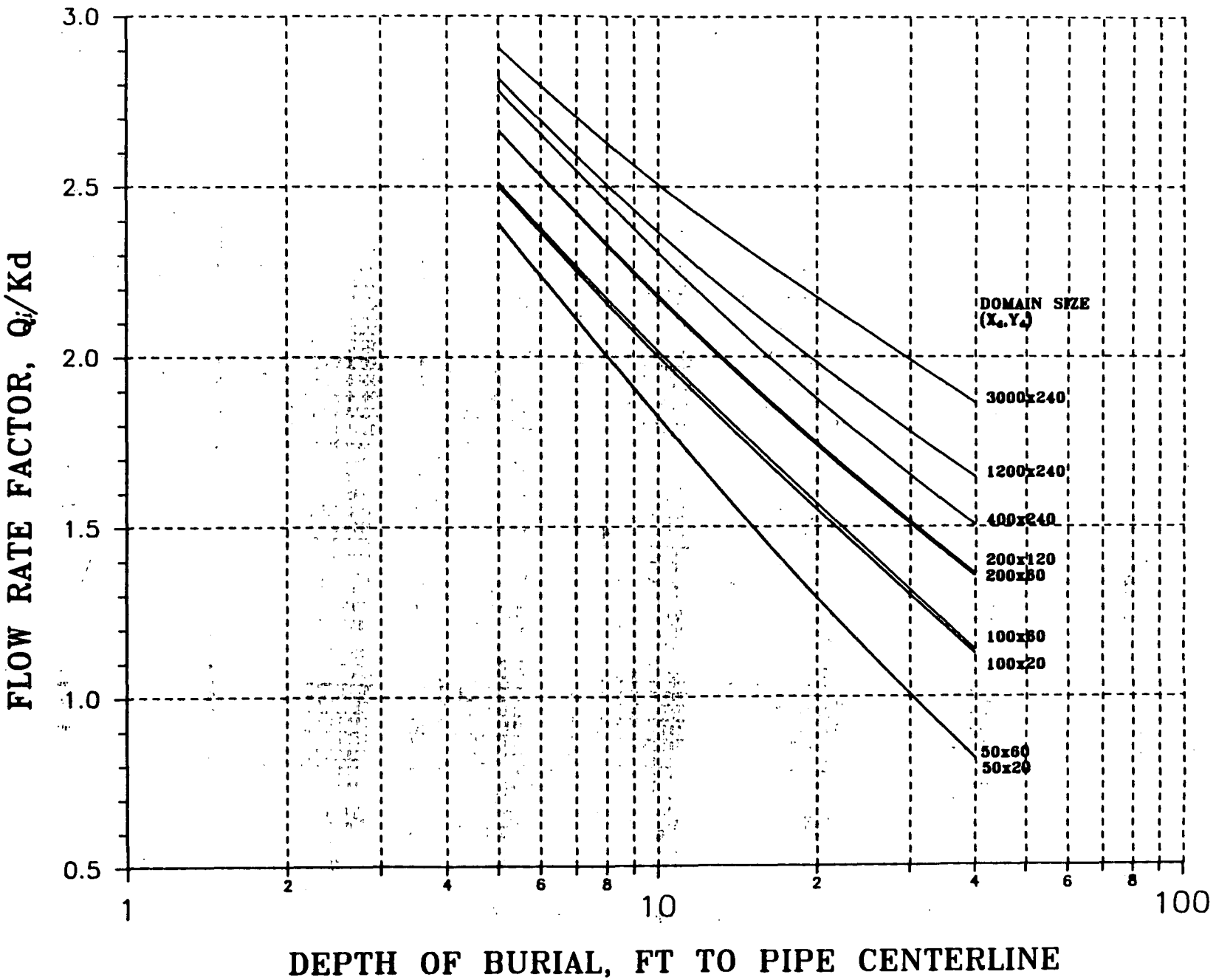

Figure 3.13b Design chart for K_x/K_y = 10 providing the required flow rate factor (Q_i/Kd_b) versus depth of burial, d_b, for various domain sizes.

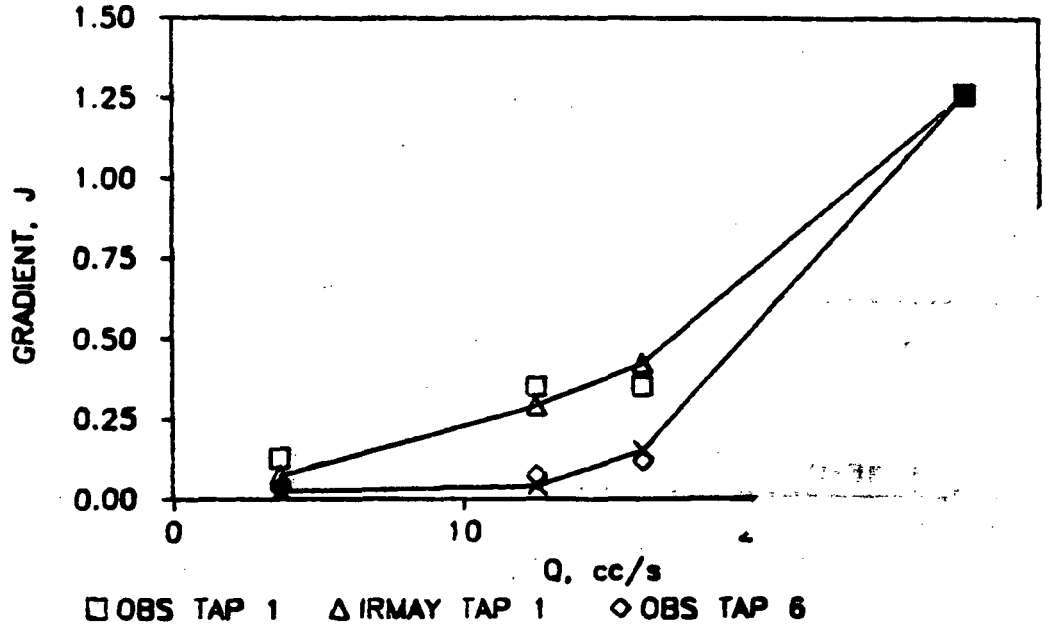

Figure A1.2 Comparison of gradient J using Irmay's equation and Roberts et al. (1986) observed data.

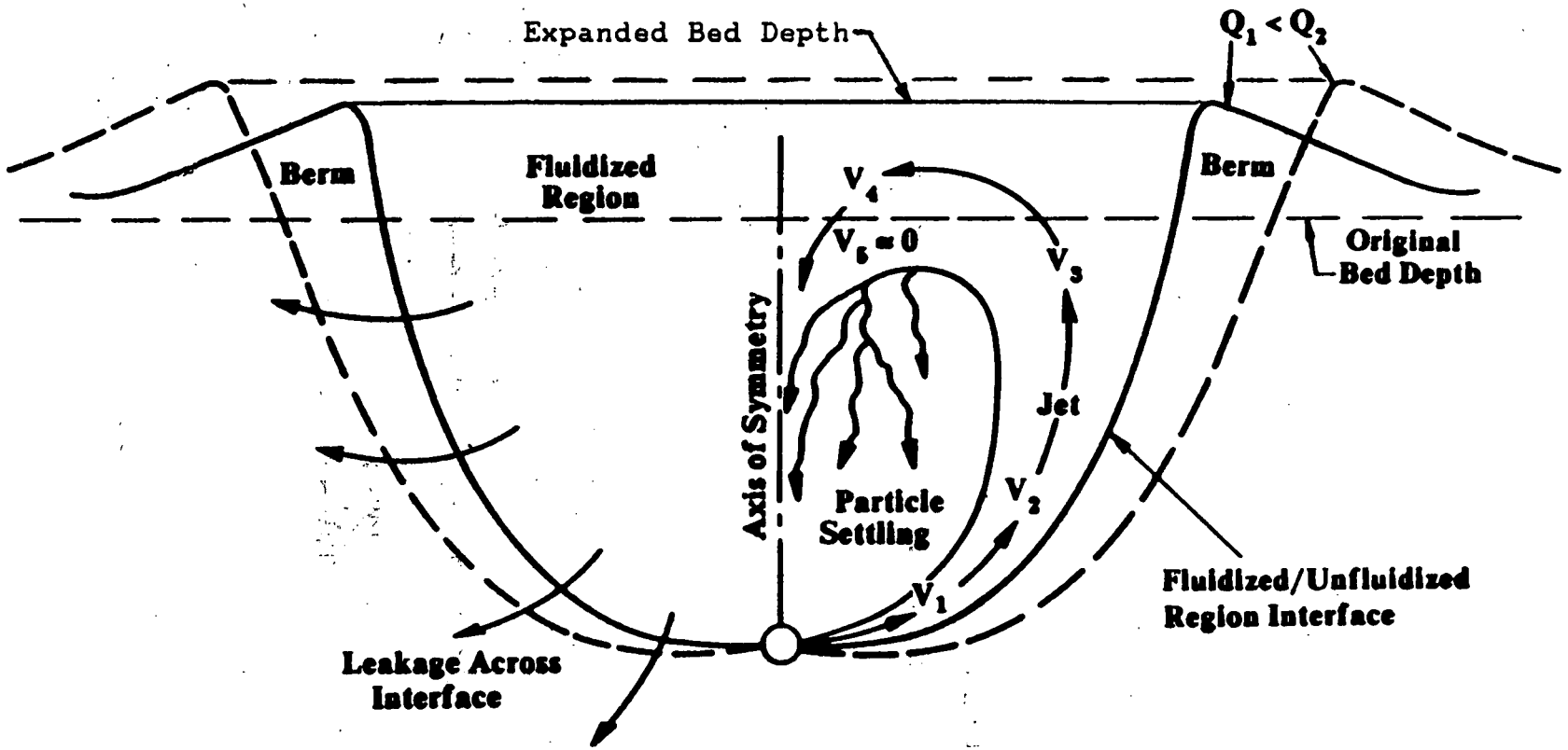

Figure A1.1 Fluidized region above a source pipe for two flow rates showing various physical processes (after Weisman et al., 1988)